An Overview of SAX99: Acoustic Measurements

Eric I. Thorsos, Kevin L. Williams, Nicholas P. Chotiros, *Associate Member, IEEE*, James T. Christoff, Kerry W. Commander, *Member, IEEE*, Charles F. Greenlaw, D. Vance Holliday, Darrell R. Jackson, Joseph L. Lopes, Duncan E. McGehee, John E. Piper, Michael D. Richardson, and Dajun Tang

***Abstract*—A high-frequency acoustic experiment was performed at a site 2 km from shore on the Florida Panhandle near Fort Walton Beach in water of 18–19 m depth. The goal of the experiment was, for high-frequency acoustic fields (mostly in the 10–300-kHz range), to quantify backscattering from the seafloor sediment, penetration into the sediment, and propagation within the sediment. In addition, spheres and other objects were used to gather data on acoustic detection of buried objects. The high-frequency acoustic interaction with the medium sand sediment was investigated at grazing angles both above and below the critical angle of about 30°. Detailed characterizations of the upper seafloor physical properties were made to aid in quantifying the acoustic interaction with the seafloor. Biological processes within the seabed and the water column were also investigated with the goal of understanding their impact on acoustic properties. This paper summarizes the topics that motivated the experiment, outlines the scope of the measurements done, and presents preliminary acoustics results. A preliminary summary of the meteorological, oceanographic, and seafloor conditions found during the experiment is given by Richardson *et al.* [1].**

***Index Terms*—Acoustic imaging, acoustic measurements, acoustic scattering, attenuation measurements, buried object detection, seafloor, sediments, synthetic aperture sonar.**

I. Introduction

IN THE FALL of 1999, a high-frequency sediment acoustic experiment, "SAX99" (for sediment acoustics experiment - 1999), was performed in shallow water about 2 km from shore on the Florida Panhandle near Fort Walton Beach (Fig. 1). The primary objective of this experiment was to quantify the interaction of high-frequency acoustic fields (mostly in the 10–300-kHz range) with the seafloor sediment, which was medium sand at the experiment site. More specifically, the goal in SAX99 was to quantify acoustic backscattering from the seafloor sediment, acoustic penetration into the sediment, and acoustic propagation within the sediment. In addition, spheres and other objects were used to gather data on acoustic detection of buried objects. The critical grazing angle at the experiment site is about 30°, and an important aspect of SAX99 was to quantify the acoustic interaction with the seafloor at grazing angles both above and below the critical angle. For propagation within the surficial sediment, topics of interest include absorption and attenuation as functions of frequency and spatial coherence of the propagating field. In order to quantify these acoustic processes, SAX99 investigators carried out detailed characterizations of seafloor physical properties. These characterizations were done chiefly in the upper half meter of the sediment, since attenuation confines high-frequency fields largely to this region. In addition, biological processes within the sediment and the water column were investigated with the goal of understanding the potential impact of these processes on high-frequency sediment acoustics.

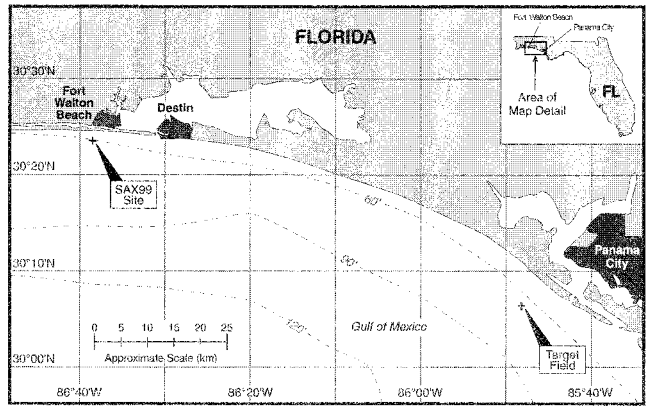

Fig. 1. Location of the SAX99 site near Fort Walton Beach, FL. Some measurements were also made at the target field near Panama City.

SAX99 has only recently been completed, and the task of analyzing the data has just begun. Nevertheless, we felt it would be useful to present an overview of SAX99 in this special issue on high-frequency acoustics to acquaint the reader with the topics that motivated the experiment, to outline the scope of the measurements done, and to indicate where the investigations might lead. The topics to be covered have been divided into two separate papers in this issue. This paper focuses on the acoustic measurements, while a paper by Richardson *et al.* [1] gives an overview of the physical and biol

ogical measurements that were made during SAX99. The separation of topics may not appear clear cut, since acoustical techniques were used to make many of the measurements discussed in [1]. However, we view the acoustical measurements in [1] as "acoustical oceanography," i.e., the use of acoustics to measure oceanographic properties. On the other hand, we will (ul-

Manuscript received January 30, 2000; revised October 10, 2000. This work was supported by the Office of Naval Research, code 321 OA (Dr. Jeffrey Simmen).

E. I. Thorsos, K. L. Williams, D. R. Jackson, and D. Tang are with the Applied Physics Laboratory, University of Washington, Seattle, WA 98105-6698 USA.

N. P. Chotiros is with the Applied Research Laboratories, University of Texas at Austin, Austin, TX 78713-8029 USA.

J. T. Christoff, K. W. Commander, J. L. Lopes, and J. E. Piper are with the Naval Surface Warfare Center, Coastal Systems Station, Panama City, FL 32407-7001 USA.

C. F. Greenlaw, D. V. Holliday, and D. E. McGehee are with BAE SYSTEMS, Analysis and Applied Research Division, San Diego, CA 92123-4333 USA.

M. D. Richardson is with the Marine Geosciences Division, Naval Research Laboratory, Stennis Space Center, MS 39529-5004 USA.

Publisher Item Identifier S 0364-9059(01)01559-X.

timately) seek to understand the "underwater acoustics" measurements described in this paper in terms of the environmental descriptions obtained independently. At present, an

alysis of the acoustical and environmental measurements is just beginning, and no attempt will be made here to model the acoustical measurements. Indeed, only a few preliminary acoustics results will be presented. Detailed analyzes of the data sets from SAX99 will be the subject of future publications.

A. Motivation: Applied Issues

The motivation for undertaking SAX99 arose from a variety of technical issues in the area of high-frequency sediment acoustics, ranging from basic to applied. A motivating applied issue is the detection and classification of objects, such as mines, buried in sediments. The character and relative strength of the returns from the buried object (dependent on the level of acoustic penetration) and from the sediment itself (dependent on the level of backscattering) will determine whether detection and classification are possible. Intriguing issues have arisen for the case of sandy sediments with sound speeds greater than the water above. If such sediments are modeled as fluids with flat interfaces, a critical grazing angle is predicted, often in the $20°–30°$ range, below which there is no appreciable acoustic penetration into the sediment except for the evanescent wave close to the interface. If this picture were correct, acoustic detection of buried objects would not be possible at grazing angles below the critical angle, except possibly in the evanescent wave region within a wavelength or two of the interface. Substantial evidence exists [2]–[5], however, for acoustic penetration into the sediment at angles below this critical grazing angle to depths deeper than reached by the evanescent wave, implying an inadequacy of the fluid–sediment, flat-interface model. Accounting for shear effects via a visco-elastic model leads to negligible changes in the compressional wave within sand sediments [6], [7]. Also, the extremely high shear wave attenuation indicates that coupling into shear waves cannot account for observed subcritical penetration. (SAX99 measurements [1] for shear wave attenuation of 30 dB/m at 1 kHz suggest [8] an attenuation of order 600 dB/m at 20 kHz.) Thus, it is important to fully understand the factors that contribute to acoustic penetration at subcritical grazing angles. In addition to the magnitude of the acoustic field penetrating into sediments, the spatial coherence of the penetrating field is important in defining the quality of images of buried objects.

Fig. 2 shows an example of a detection of a buried cylinder (center of figure) at an incident grazing angle well below the critical angle. (The feature in the lower left of the figure is a marker left by divers.) This image was obtained with a synthetic aperture sonar (SAS) system operated by the Coastal Systems Station (CSS) in Panama City, Florida. The SAS measurements that were made in conjunction with SAX99 will be discussed later in this paper, and Fig. 2 is presented here simply to illustrate the reality of subcritical-angle detections. SAS measurements were made both at the SAX99 site and at the target field near Panama City (see Fig. 1). For the measurement shown in Fig. 2, the frequency was 20 kHz, the top of the target cylinder was about 50 cm below the sediment surface, and the incident

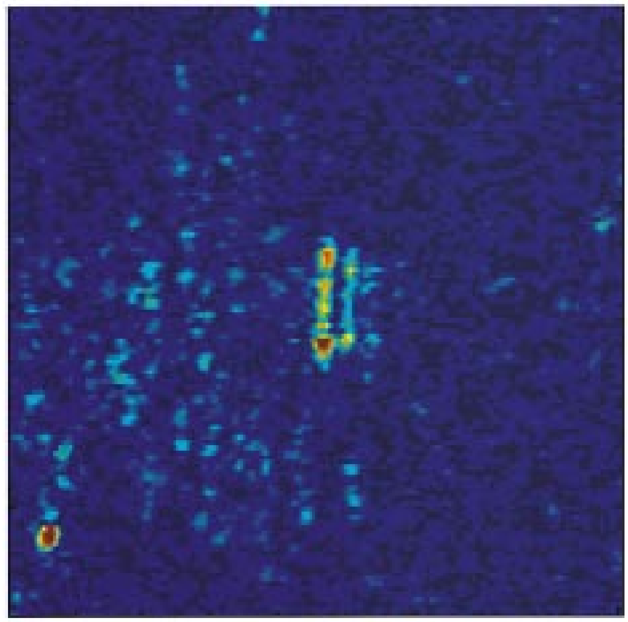

Fig. 2. SAS image of a buried target obtained by CSS. The frequency was 20 kHz, the top of the target cylinder was about 50 cm below the sediment surface, and the incident grazing angle was $4°$ to $5°$ compared to a critical angle of about $30°$.

grazing angle was $4°$ to $5°$ compared to a critical angle of about $30°$.

B. Motivation: Basic Research Issues

An improved understanding of the coupling of sound into sediments, of the propagation and attenuation within the sediment, and of the scattering from the sediment interface and from interior heterogeneity should lead to improved models for predicting when buried objects can be detected and classified. Ocean experiments are necessary to reliably address these issues because of the near impossibility of reproducing realistic ocean sediment conditions in the laboratory. These sediment conditions include surface roughness, volume heterogeneity, effects of bioturbation, and the arrangement of grains under natural sediment deposition conditions.

For the topic of subcritical acoustic penetration, SAX99 was designed to quantify the role of at least three mechanisms as possible contributors: 1) the porous nature of the sediment that could lead to a second slow compressional wave [2]; 2) roughness of the water/sediment interface that could diffract or refract energy into the sediment [9], [10]; and 3) volume heterogeneity within the sediment that could scatter the evanescent wave (propagating along the water–sediment interface) into the sediment. Experimental data acquired both in the field and in the laboratory have been interpreted [2] using a poro-elastic solid model for the sediment according to Biot's theory. This approach can yield a slow compressional wave with a wave speed less than the speed of sound in water, and thus no critical angle exists for that wave. However, it has been shown that the results from experiments carried out to date could also be explained as a result of roughness at the sediment–water interface [10]. Furthermore, recent modeling results [11], [12] show sediment volume heterogeneity near the water–sediment interface (within about a wavelength of the interface) could also cause significant subcritical penetration under some conditions.

Recently, additional measurements and analyses suggest the importance of seafloor roughness as a mechanism for subcritical penetration. Simpson and Houston [13] reported laboratory measurements in which the penetrating field increased markedly when the interface was deliberately roughened. Schmidt and Lee [14] used simulations to show that ripple fields could couple substantial subcritical energy into the sediment. Maguer *et al.* [5] made measurements in the 2–15-kHz range, and argued, based on modeling studies, that the subcritical penetration they observed below 5–7 kHz is due to the evanescent wave, while above 5–7 kHz it is due to rough surface scattering. These conclusions were strengthened by very recent analyses [15], [16]. Though arguments are accumulating on the importance of seafloor roughness for subcritical acoustic penetration, seafloor characterization has not been extensive in previous acoustic measurements. Consequently, it still is not known if other mechanisms contribute.

In the context of detecting and classifying buried objects, sediment backscattering issues bear on the important task of accurately modeling the interference due to seafloor reverberation. In order to have reliably accurate models of this interference, the underlying scattering mechanisms need to be understood. However, for backscatter and general bistatic scatter from sediments at high frequencies, questions persist on the identity of the dominant scattering mechanisms and the frequency range that are they important. Possible scattering mechanisms include interface roughness, volume heterogeneity, discrete scatterers, bubbles, and, at very high frequencies, sediment grains.

While the level of acoustic penetration into sediments and the level of backscattering from sediments are important, SAX99 also addressed a broader range of technical issues associated with scattering from sediments, propagation and attenuation within sediments, and scattering from buried objects. Some of these issues are summarized in the following paragraphs.

In addition to understanding sediment scattering levels, it is important to understand the spatial variability of such scattering, and the temporal dependence due to biological and hydrodynamic reworking of the sediment. For volume scattering, discrete scatterers, such as shells, may also be important. How such discrete scattering should be treated in the context of stochastic modeling remains an issue. The importance of fine-scale stratification and sound speed gradients for modeling bottom interaction at high frequency also needs to be better understood. At a fundamental level it is not known if sediment interface scattering can be adequately represented by a fluid–sediment approximation, or if it is necessary to resort to a Biot representation. Furthermore, the importance of multiple scattering also needs to be clarified.

Some aspects of sediment acoustics can only be modeled (aside from empirically) by going beyond the relatively simple fluid model description: these include absorption versus frequency and the corresponding velocity dispersion. It is still not known if this frequency dependence can be predicted by the Biot model (e.g., see Stoll [17]) or other models when a broad range of sediment characterization is used that highly constrains the acoustic model predictions. One potential complication to such a comparison is that within the framework of the Biot model, volume heterogeneity might lead to coupling into rapidly attenuating slow waves which may appear simply as increased fast wave absorption [18]. Thus, knowledge of volume heterogeneity may be important in this context. [Note: The term "attenuation" is used here to include both the effects of absorption and scattering in reducing the intensity of a propagating wave.]

At grazing angles well above the critical angle, a substantial fraction of the sound incident on the seafloor will penetrate the interface. The ability to use such fields to image buried objects may be limited by forward scattering from the rough water–sediment interface and from volume heterogeneity within the sediment. Such scattering will degrade the spatial coherence of the field as well as distort and spread in time the waveform of the propagating pulse. A need exists to better understand the magnitude of these effects and their frequency dependence. In particular, the ability to reliably model these effects from knowledge of sediment structure needs to be developed.

C. Environmental Characterization

The physical and biological measurements made during SAX99 are described in [1]; in this section a brief description is given from an acoustics perspective. In general terms, the goals were to measure the acoustically important mean properties of the sediment as functions of depth, to measure the spatial variability of the sediment that leads to scattering, to monitor the temporal variability of the sediment (for correlation with temporal variability of scattering), and to understand biological and hydrodynamic processes that may affect the spatial and temporal variability of the sediment.

An important focus regarding sediment mean properties was to define as completely as possible the parameters that enter into a Biot model description of the sediment. Measurements included porosity, permeability, compressional and shear speeds and attenuations to infer the frame bulk and shear moduli, and microscopic measurements to define the tortuosity and the pore size parameter. In addition to these direct measurements, low-frequency sediment propagation measurements were made in order to look for velocity dispersion, a prediction of Biot theory.

Characterizing the physical environment for high-frequency acoustic scattering is a challenging task. In order to understand scattering, measurements of mean sediment properties are not sufficient, and it is necessary to measure the spatial variability of certain sediment properties to a resolution of about a quarter of an acoustic wavelength. This variability is manifest in the water–sediment interface roughness and sediment volume heterogeneity, i.e., sound speed and density spatial variations. The goal in SAX99 was to measure the sediment spatial variability to a resolution of about 1 cm (or better for some measurements). If later data analysis shows this resolution has been achieved, the sediment variability will be adequately characterized for scattering processes up to frequencies of about 45 kHz. For higher acoustic frequencies the sediment characterization based directly on measurements will not be as complete. However, quarter-wavelength resolution of sediment variability is only necessary for understanding acoustic backscattering from sediments. Forward scattering is sensitive to larger scale sediment variability, relaxing the resolution requirement, or, equivalently, increasing the upper frequency range that can be addressed quantitatively.

The temporal change of interface roughness and volume heterogeneity is of interest for understanding the effects of biological processes as well as of wave and current forcing on high-frequency sediment scattering and penetration. Temporal changes were monitored with acoustic scattering measurements over extended periods and with studies of interface roughness and volume heterogeneity change over time.

II. Overview of SAX99

A. Site Selection Considerations

A primary consideration for selecting an experiment site for SAX99 was a need for the seafloor to have a relatively high critical angle (e.g., $25°–30°$) in order to allow study of acoustic penetration and scattering both above and below the critical angle. This requirement translates into a sediment-to-water sound speed ratio greater than about 1.1, which implies that the seafloor sediment should be sand. Because experiment plans called for hydrophones to be inserted into the top meter of the sediment, a surface sand layer 1 m deep was considered a requirement.

A description of the site surveys used to select the final site can be found in [1]. Initially, a site near Panama City had appeared promising (a region including the target field in Fig. 1), but further investigation revealed that mud inclusions (or mud lenses) were more common there than at the site near Fort Walton Beach, and the latter site was finally selected. Prior to final site selection, CSS investigators had buried target cylinders at the Panama City site in April 1999 to allow a substantial period for sediment recovery after burial. Therefore, a limited number of measurements were also made at the Panama City site.

B. The SAX99 Site

The final site was selected in 18–19 m of water about 2 km from shore near Fort Walton Beach, Florida. Fig. 3 shows the location of the major measurement areas used during SAX99, but many other areas were also used as part of the environmental characterization. In this paper, acoustic measurement activity will be described that occurred at the APL, BAMS, XBAMS, ARL, and CSS areas, and part of the activity at the BAE SYSTEMS tower area will also be covered. Measurement sites not treated in this paper are covered in [1]. Fig. 3 was obtained with an EM 3000 multibeam echosounder (R. Flood, SUNY), which is also discussed in more detail in [1].

The SAX99 site satisfied the essential requirements needed for the planned acoustic measurements. The sediment critical angle is about 30° at the site. The sand layer at the sediment surface is close to 1 m in depth or greater. However, shell fragment layers were encountered in some areas within the top 1 m of sediment, and whole sand dollars (generally dead) were also observed within the sediment, usually below about 20 cm depth. A sediment ripple field was present at the site, with wavelengths generally in the 50–70-cm range. The ripple amplitude

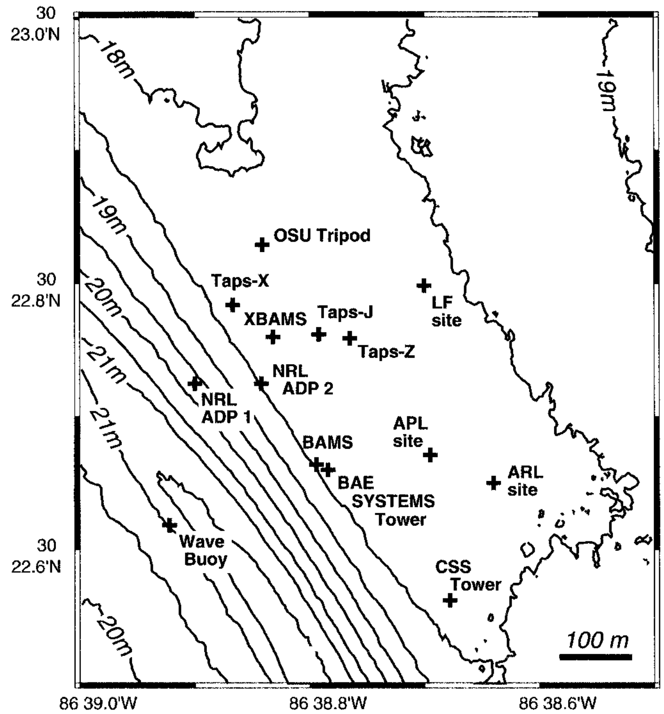

Fig. 3. Location of the major measurement areas during SAX99. The position of the moored R/V Seward Johnson was to the west of the ARL site and to the south and slightly west of the APL site.

varied during the course of SAX99, but was in the 1–3-cm range (mean to peak). See [1] for further discussion of the properties of the SAX99 site.

C. Brief Chronology of SAX99

The R/V Tommy Monro initiated activity during the Sept. 28–30 period with site survey and low-frequency work. The R/V Pelican arrived at the SAX99 site on Oct. 2 and left on Oct. 28. During this period, eight round trips were made between a staging area at the CSS dock in Panama City and the SAX99 site, and each trip brought additional investigators and equipment to the SAX99 site. One of these trips to CSS (Oct. 7–10) was forced by high seas at the SAX99 site. The R/V Pelican supported a continuous stream of equipment deployments and small boat/diving operations throughout its stay at the SAX99 site. The Pelican also deployed the four moorings used by the Seward Johnson.

The R/V Seward Johnson arrived at the SAX99 site on Oct. 14 and left on Nov. 14. It went into a four-point moor on Oct. 16 and came out on Nov. 11. During this period, the R/V Seward Johnson supported a variety of diver-intensive acoustic and environmental measurements, and as many as 20 cables were deployed from ship to equipment on the bottom. Only once (Oct. 31–Nov. 2) did high seas force these cables to be disconnected and dropped to the bottom. The R/V Seward Johnson then temporarily came out of the four-point moor, and transited to CSS to wait out the high seas. The ship returned to the SAX99 site on Nov. 2, came back into the moor on Nov. 3, followed by cable recovery that day and a resumption of experiments.

Finally, the R/V Mr. Offshore was at the SAX99 site on Oct. 28 to support CSS SAS measurements.

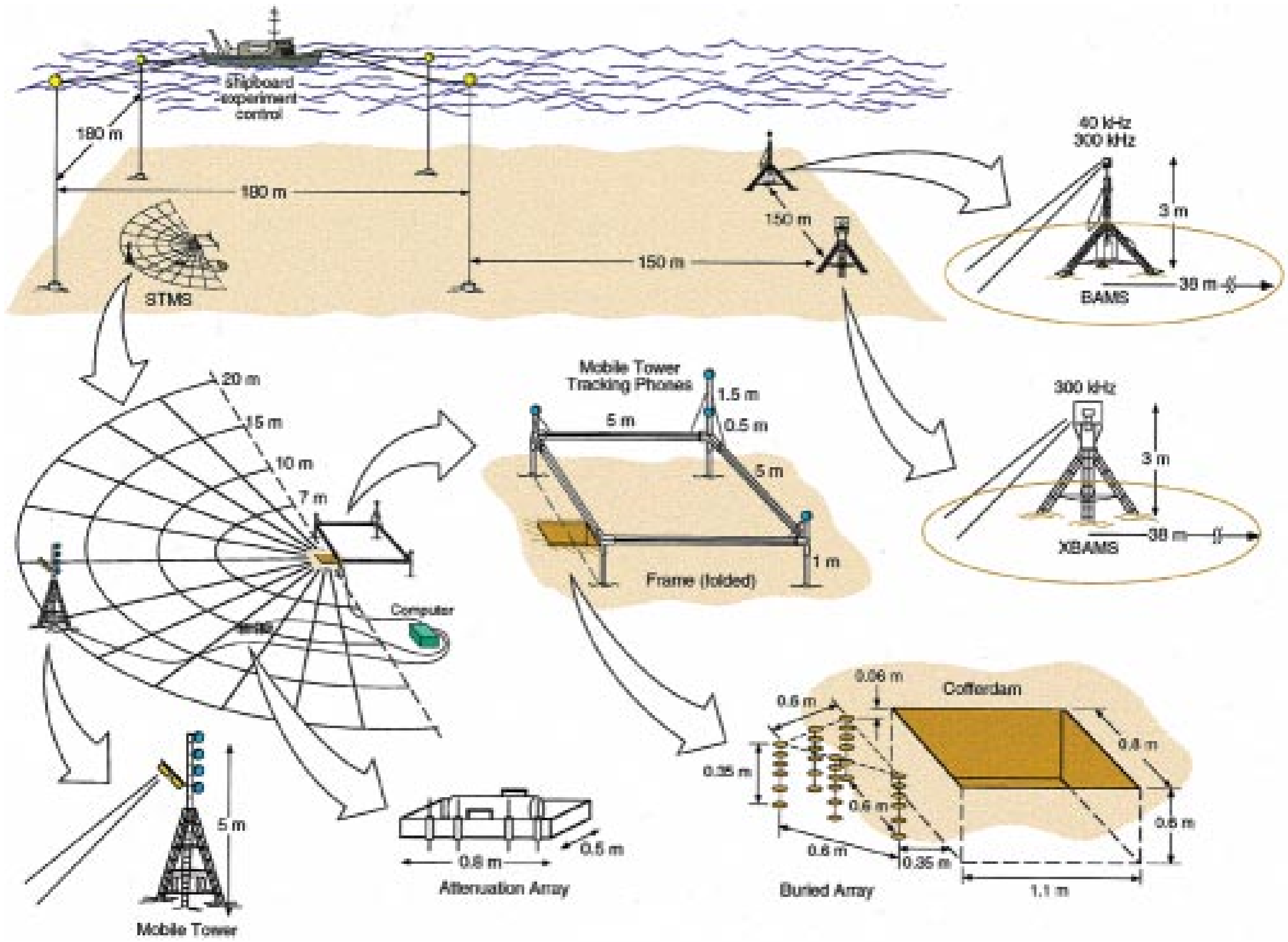

Fig. 4. The spatial arrangement of APL-UW equipment during SAX99: the Benthic Acoustic Measurement System (BAMS), the Accelerated Benthic Acoustic Measurement System (XBAMS), and the Sediment Transmission Measurement System (STMS). Simplified diagrams of STMS subsystems are shown in the figure, and details of each system are given in the text.

III. APL:UW Experiments During SAX99

The participation of the Applied Physics Laboratory of the University of Washington (APL-UW) in SAX99 was directed toward a better understanding of acoustic scattering from ocean sediments and of acoustic penetration into and propagation within these sediments. Recent work at APL-UW has examined high-frequency backscattering from ocean sediments [19] and the possible role of scattering from sediment roughness in explaining acoustic penetration at subcritical grazing angles [10].

A. Experiment Overview

Fig. 4 illustrates the equipment location relative to the mooring layout of the R/V Seward Johnson and gives simplified diagrams of the apparatus.

The Benthic Acoustic Measurement System (BAMS) [20], [21] and the Accelerated Benthic Acoustic Measurement System (XBAMS), which is similar to BAMS, collected backscattering data autonomously from circular areas 75 m in diameter over the duration of the experiment. However, the effective diameters were 36 m in order to avoid contaminating effects of sea surface scattering. BAMS operates at 40 and 300 kHz and XBAMS operates at 300 kHz. In addition to collecting data on backscattering from unperturbed areas of the bottom, localized "treatments" were carried out in the field of view of BAMS and STMS by APL-UW and NRL-SSC researchers to examine the effects of biological activity, sediment structure, and discrete scatterers on backscattering. The backscattering data set and some of the treatments are described in Section III-B. Other treatments are described in [1].

The Sediment Transmission Measurement System (STMS) was newly constructed for SAX99 and used to carry out a variety of measurements under real-time user control. These included attenuation measurements in the 80–300 kHz range, backscattering measurements in the 10 to 150 kHz range, and penetration measurements at multiple grazing angles and frequencies from 10 to 50 kHz. STMS is comprised of a diver movable tower, a large (5 m $\times$ 10 m $\times$ 1 m) frame, 30 small receivers that make up an in-sediment array, a cofferdam, a diver-held attenuation array, acquisition and control electronics, and power and communication cables to a shipboard computer. Not shown in Fig. 4 are an underwater battery pack and an RF buoy deployed for operation in the event that the STMS cables had to be disconnected from the ship.

The STMS tower was instrumented with four ITC 1032 spherical sources for penetration measurements and with an Engineering Associates (EA) model 33 planar array source and a EA model 41 source/receiver for backscatter measurements. The 30 small receivers (B&K 8103s) for the in-sediment array were implanted horizontally into the sediment from the cofferdam in order not to disturb the water–sediment interface above them. The bottom-mounted frame could be unfolded to its full 5 m $\times$ 10 m horizontal extent to protect a 5 m $\times$ 5 m region of the bottom on the tower side of the cofferdam from accidental disturbance during diver operations. The unfolded position was also used to suspend an array of four ITC 1032s, used as sources, to determine the precise positions of the 30 in-sediment array elements using acoustic surveying techniques. During acoustic penetration experiments the frame was in the folded configuration with a horizontal extent of 5 m $\times$ 5 m (as shown in Fig. 4) and used to mount the same four ITC 1032s, as receivers in this configuration, for tracking the location of the mobile tower. Four ITC 6148s (two acting as sources and two as receivers) were mounted on a small 0.8 m $\times$ 0.5 m) diver-held frame for insertion into the sediment at multiple locations to measure sediment sound speed and attenuation as a function of frequency.

B. Backscattering Measurements

1) Backscattering from Natural Sediment: For bottom scattering it is not always easy to obtain scattering from many independent areas on the bottom so that averages can be taken. The backscattering transducers for the STMS mobile tower are on the opposite side from four spherical transducers used for penetration measurements (see Fig. 4) and produced backscattering data from 10 to 150 kHz. Repositioning of the tower by divers gave measurements over independent patches of the bottom that can be intensity-averaged to obtain backscattering strengths. The sonars on BAMS and XBAMS rotate in azimuth in steps of the horizontal beam widths, which are small (5° for BAMS at 40 kHz and 1° for BAMS and XBAMS at 300 kHz). A full 360° rotation (or "scan") takes approximately 6 minutes to complete for BAMS at 40 kHz and for XBAMS (300 kHz) and approximately 30 minutes for BAMS at 300 kHz. Thus, the ensemble averages of backscattered intensity that are needed for backscattering strengths can be obtained without diver intervention.

Backscattering measurements with the mobile tower required extensive diver activity. In conjunction with penetration measurements, the mobile tower was placed by divers near the intersections of the radial lines and semicircles shown in the bottom left part of Fig. 4 with the backscattering transducers pointed away from the frame. Backscattering data were acquired for 33 positions of the mobile tower on this grid (where the 7-, 10-, and 15-m-radius semicircles intersect the solid radial lines in Fig. 4). The data set at each position included as many as nine transmissions at each of 15 center frequencies (10–150 kHz in 10-kHz increments with approximately 2-kHz bandwidth, except at the lowest two center frequencies that had bandwidths of about 1 kHz) taken 1 s apart. The multiple transmissions allowed coherent averaging to reduce the effects of scattering from fish, which were sometimes present in the field of view. A substantial number of additional backscattering measurements were made independent of the penetration studies.

Fig. 5 shows backscattering strengths as a function of grazing angle calculated from a single scan of XBAMS (Oct. 13) and BAMS (Oct. 15) at 300 kHz, a single scan of BAMS (Oct. 6) at 40 kHz, and from the 40-kHz backscattering transmissions of STMS at the 20 mobile tower locations occupied on Oct. 26. [The data below 10° are contaminated by scattering from the air/water interface due to sonar side lobes. The upper range of about 21° for BAMS and XBAMS is determined by the beam widths and tilt angles for these systems.] The scattering strengths at 300 kHz from BAMS and XBAMS are within 3 dB of each other. The scattering strengths at 40 kHz from BAMS and STMS are within about 1 dB in the overlap area near a grazing angle of 20°. This initial comparison gives some confidence that the scattering strengths being obtained are independent of the system used (as they should be). Furthermore, the large difference in scattering strength between 40 and 300 kHz is a result that will be a clear test of acoustics models when model predictions are made using the results of the SAX99 environmental characterization. Further checks on frequency dependence will be possible using other data from STMS and data from ARL-UT, CSS, and BAE SYSTEMS.

As more data sets of backscattering strength are examined, and as environmental data on sediment roughness, sediment volume heterogeneity, and sediment mean properties become available, modeling of the backscattering will be used as a key avenue in addressing fundamental questions on scattering mechanisms. The 40-kHz BAMS data can also be used to examine temporal changes in backscattering, including the effect of a significant weather event over the Oct. 31–Nov. 2 period. Over the time period Oct. 6–Nov. 4, 878 40-kHz scans were acquired. From Oct. 6 to Oct. 24 at 16:30 local time (CDT) a scan was performed once every 90 min. From that point until 16:00 on Nov. 4 (CST) a scan was performed once every 30 min.

In addition to scattering strength computation, the BAMS 40-kHz data can be used to produce images of the backscattered intensity [22]. The horizontal beam width of the 40 kHz transmitter/receiver is 5°, which implies an azimuthal resolution of about 1.1 m at a range of 12.5 m. The bandwidth of the transmission was 2 kHz and therefore the highest range resolution of the 40-kHz system is about 0.37 m. Backscattered intensity images were formed with a "pixel" size at 12.5 m of $1.1\ \mathrm{m} \times 0.5\ \mathrm{m}$. The azimuthal dimension of a pixel changes linearly with range based on the horizontal beam width, e.g., at 10 m it is 0.9 m while at 30 m it is 2.6 m. Ninety-degree sectors from two such images are shown in the following subsection to illustrate effects of the localized treatments carried out in the field of view of BAMS. Images of bathymetry [23] and temporal changes in scattering can also be made [24] and will be examined, along with images of backscattered intensity, in investigating spatial and temporal variations in bottom backscattering.

XBAMS carried out 204 scans between Oct. 6 and Oct. 31, whereupon the system shut down due to low battery voltage. XBAMS scans were carried out once every 3 h, and images similar to those formed with the BAMS 40-kHz system will be formed using these data. Only five BAMS 300-kHz scans were completed before a hard disk error on Oct. 18 prevented further data acquisition. However, this data set is still valuable (e.g.,

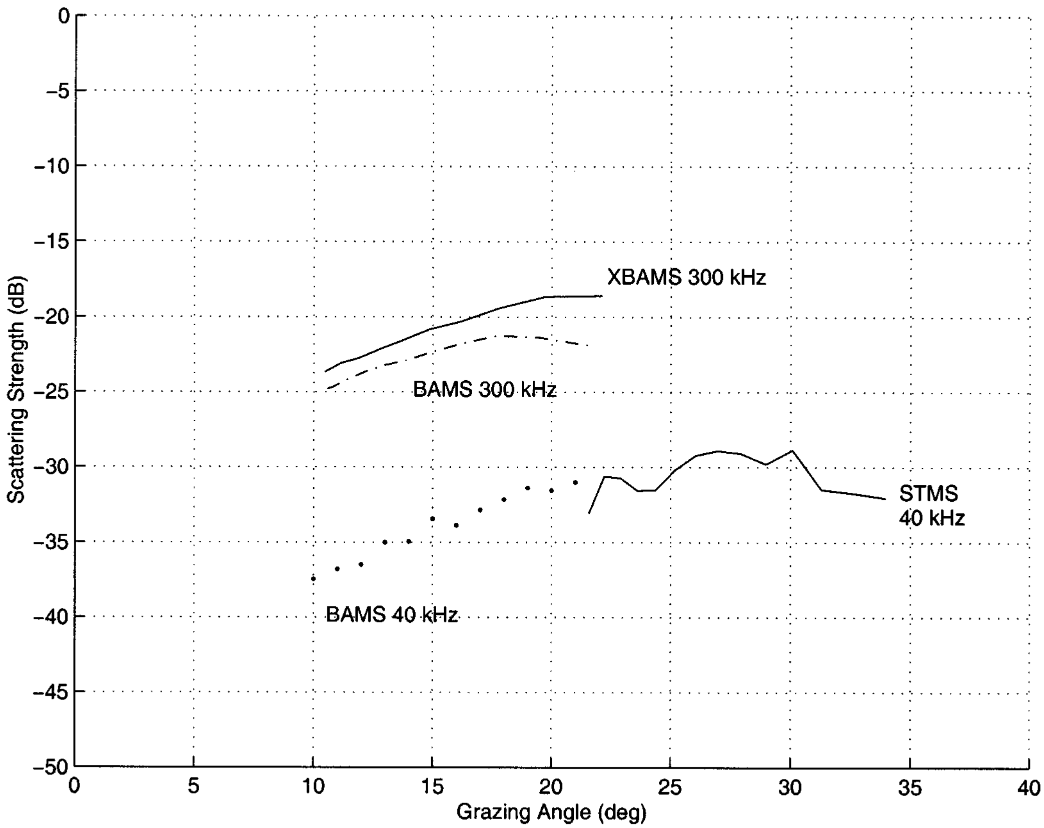

Fig. 5. Backscattering strength as a function of grazing angle calculated from a single scan of XBAMS and BAMS at 300 kHz, a single scan of BAMS at 40 kHz, and 40-kHz STMS backscattering transmissions at 20 mobile tower locations occupied on Oct. 26.

Fig. 5) for comparison to backscattering strengths determined with XBAMS at 300 kHz.

2) Backscattering from Sediment Treatments Areas: Specific, well-defined treatments (or manipulations) of the seafloor (Tables I and II) were conducted by NRL in the field of view of BAMS and by NRL and APL-UW in the field of view of the STMS tower in order to assess the impact of changes in seafloor roughness and the role of near surface discrete scatterers on high-frequency scattering from the seafloor. Biological and physical processes operating at the benthic boundary layer are known to alter surficial seafloor physical properties and bottom roughness [25]–[27]. These changes often have profound effects on the magnitude (and on the temporal and spatial fluctuations) of backscattering of high-frequency acoustic energy from the seafloor [19], [24], [28]. Larger discrete scatterers, such as shells, can also influence and sometimes dominate acoustic backscattering at or near the seafloor [26], [29]–[31]. Creating a well-defined roughness by raking the seafloor or the introduction of spherical discrete scatterers (marbles) was not meant to mimic natural conditions but to provide acoustic model validation and determine acoustic system sensitivity. Model simulations of the potential effects of roughness [28] and discrete scatterers (using a model similar to that in [29], [30]) were used as a guide in planning the manipulative experiments.

Before manipulations began, 2 m $\times$ 2 m areas were marked off with plastic tent stakes and #18 Nylon Mason Twine. Five such areas were set in the NE quadrant of the circular area associated with the BAMS tower and two areas were located within the acoustic field of view of the STMS tower. The sides of each treatment area were either parallel or orthogonal to the radial acoustic beams, and for BAMS the areas were centered at 12.5 m from the central vertical axis of the acoustic tower and separated by 2 m of open seafloor. Precise pixel locations of the 2 m $\times$ 2 m treatment areas relative to the BAMS coordinate system were determined by placing 0.2-m-radius liquid filled target spheres directly beyond each treatment area. The target spheres provided high target strength markers for the sites of the manipulation experiments. After removal of the target spheres the treatment areas were acoustically indistinguishable from the surrounding area suggesting that manipulations by divers or presence of the marking systems had little effect on acoustic backscattering strength. Three types of manipulations were conducted within the treatment areas. Roughness was alternately created and destroyed using hand-held plastic drywall knives. A sawtooth pattern at $45°$ pitch was cut from the business end of a plastic drywall knife that allowed divers to create ripples (19.5 mm wavelength) within treatment areas #4 and #5 [Fig. 6(a)]. This ripple wavelength is about half the acoustic wavelength of the 40 kHz BAMS transducer, and is the ideal "Bragg" wavelength for low grazing angle backscattering. Treatment areas #4 and #5 were alternately smoothed or raked either parallel or orthogonal to the acoustic path from the BAMS tower. At treatment sites #1 and #3 glass spheres (marbles) were placed in a random pattern at increasingly dense

TABLE I
A SUMMARY OF NRL SEAFLOOR MANIPULATIVE EXPERIMENTS CONDUCTED NEAR THE BAMS TOWER (OCT. 22–NOV. 7). STEREO AND DIGITAL PHOTOGRAPHS OF THE TREATMENT SITES WERE TAKEN ON OCT. 19 BEFORE SEAFLOOR MANIPULATIONS AND ON OCT. 22, 23, 26, 27, 29 AND NOV. 4 1999 AFTER SEAFLOOR MANIPULATIONS. FIG. 7 INDICATES WHERE THE FIVE MANIPULATION AREAS WERE RELATIVE TO BAMS

Area # Treatment	5 Raking	1 Large Marbles	2 Shells	3 Small Marbles	4 Raking
Oct. 22	Orthogonal	Flatten	—	Flatten	Smooth
Oct. 23	Smooth	60	—	60	Parallel
Oct. 24	—	250	—	250	—
Oct. 26	Parallel	500	81 large Convex	500	Smooth
Oct. 27	Smooth	750	81 large Concave	750	Orthogonal
Oct. 27	—	1000	200 small 81 large	1000	—
Oct. 29	Orthogonal	Remove	200 small 81 large	1000	Smooth
Oct. 30	Smooth	61	200 small 81 large	1000	Parallel
Oct. 31	Parallel	310	200 small 81 large	1000	Smooth
Nov. 3	Smooth	560	200 small 81 large	1000	Orthogonal
Nov. 4	Parallel	Bury (surface)	Remove	2118	Parallel
Nov. 5	Orthogonal	Bury (5 cm)	—	2118	Orthogonal

TABLE II
A SUMMARY OF NRL SEAFLOOR MANIPULATIVE EXPERIMENTS CONDUCTED NEAR THE APL STMS TOWER (NOV. 11–12)

Area # Treatment	1 Rake/Shells	2 Rake/Marbles
Nov. 9	Smooth	Smooth
Nov. 9	Orthogonal	Orthogonal
Nov. 9	Parallel	Parallel
Nov. 9	Orthogonal	Orthogonal
Nov. 10	200 small and 81 large shells	64
Nov. 10	Remove Shells	250
Nov. 10	—	500
Nov. 10	—	750
Nov. 10	—	1000

concentrations [Fig. 6(b)]. The smaller (10-mm-diameter) glass spheres were too small to be recovered but the larger (35-mm-diameter) yellow cat's-eye marbles were removed midway through the experiments and the increasingly dense concentration pattern repeated. Near the end of the experiments, the larger marbles were buried flush to and then below the sediment surface. Mollusk shells of various sizes and concentrations were placed within treatment area #3. The mollusk shells were never exposed to air during collection or subsequent manipulation. Digital photographs were taken to document treatments and stereo photographs were collected to determine seafloor roughness. Similar manipulations were later conducted at two treatment sites within the field of view of the STMS tower, but with the center of the treatment areas 5.8 m from the central vertical axis of the tower. Since this much lighter tower could be moved by divers, alternate ensonifications (with the same pulses used for the backscattering data described above) and manipulations were done at the two treatment sites approximately 180° apart relative to the tower. Marbles in the mobile tower experiments were 19.0 mm in diameter and the mollusk shells and drywall knives were the same

(a)

(b)

Fig. 6. Photographs of two of the 2 m $\times$ 2 m treatment sites during the manipulative experiments near the BAMS tower. (a) Treatment site #5 with seafloor raked orthogonal to the acoustic path from the BAMS tower. (b) Treatment site #1 with 750 large (35-mm-diameter) "cat's-eye" marbles.

employed during the manipulative experiments near the BAMS tower.

Preliminary results from two 40-kHz scans in a treatment area made from the BAMS tower are shown in Fig. 7. The scattered intensity in Fig. 7 is presented in terms of a Lambert parameter [24] for each pixel, which normalizes the intensity in a way that reduces its range dependence. First, the scattered intensity is normalized by the incident intensity and the ensonified area, and effects of transmission loss and beam loss are removed. [At this stage, an ensemble average of the normalized scattered intensity would yield the (dimensionless) scattering cross section per unit area per unit solid angle.] The scattered intensity is further normalized by a factor of $\sin^2\theta$, where θ is the grazing value, to obtain the Lambert parameter for each pixel. The top panel of Fig. 7 shows pre-treatment backscattering levels at five treatment sites, and the bottom panel of Fig. 7 shows the levels after the second set of treatments of Oct. 27. [The higher backscattering level in the region beginning about 3 m north of treatment area #5 is due to NRL's *in situ* resin impregnation system.] After treatment, four of the five sites had higher scattering levels than before; treatment area #5 had been recently smoothed and gave low backscattering levels. Backscattering from glass spheres was found to follow a predictable pattern. The highest backscattering levels came from treatment area #1, which contained 1000 35-mm-diameter glass spheres, while treatment area #3 had 1000 10-mm-diameter glass spheres and showed an expected reduction in backscattering level in comparison to area #1. Other measurements with glass spheres showed an expected increase in backscattering level with higher sphere concentrations. The second highest backscattering levels occurred in treatment area #4, which was prepared by raking orthogonal to the acoustic path from BAMS. After treatment, the backscattering level at area #4 was much higher than before treatment, while raking parallel to the acoustic path (not shown) had little impact on the backscattering level. Treatment area #2 had 281 mollusk shells which led to much higher scattering levels than background sites, suggesting that concentrations of shells encountered in nature can also greatly increase acoustic scattering strength. The preliminary results in Fig. 7 suggest that observed and modeled backscattering levels should agree at least qualitatively. Quantitative comparisons of this data with acoustic models are being carried out as part of ongoing investigations.

Backscattering at treatment areas also provided important information on the effects of biological reworking of the sediment. It was found that the increased values of backscattering strength in orthogonally raked treatments rapidly decayed, which correlates with visual observations of the rapid decay of diver-made roughness as a result of sediment reworking by fish and larger megafauna. The decay of the backscattered intensity, as indicated by the Lambert parameter for the treatment site, is shown in Fig. 8. It follows from the curve fit in Fig. 8 that the characteristic time for the decay (i.e., the time for the backscattered intensity to decrease by a factor of e) is about 10 h. After about one day, values of acoustic backscattered intensity were nearly the same as pre-treatment levels, and after two days the diver-made roughness was difficult to visually detect.

C. Penetration Measurements

Numerical simulations (using methods described in [10]) indicated that an array of 18 buried hydrophones, in the nominal configuration shown in Fig. 4 (the three vertical columns farthest from the cofferdam), would give sufficient resolution in penetration experiments to distinguish between possible penetration mechanisms. However, the addition of 12 more hydrophones allowed even better resolution. The strategy implemented during the experiment was to initially deploy 18 hydrophones, acquire data for several days, then deploy the last 12 and acquire additional data. The penetration experiment used several of the STMS subsystems: the mobile tower, the frame, the tracking phones, the cofferdam, the buried array, and the computer.

The frame was deployed first and served several purposes as described in Section III-A. It was deployed in its 5 m $\times$ 5 m folded mode from the fantail of the R/V Seward Johnson at a site that divers had inspected. Divers oriented the frame such that the ridges and troughs of the large scale ripple field made an angle of about 55° relative to the side of the frame immediately above the cofferdam (see Fig. 4). This orientation placed the legs of the frame in the troughs of the ripple field. Divers also leveled the frame at this time. The frame had two vertical guides

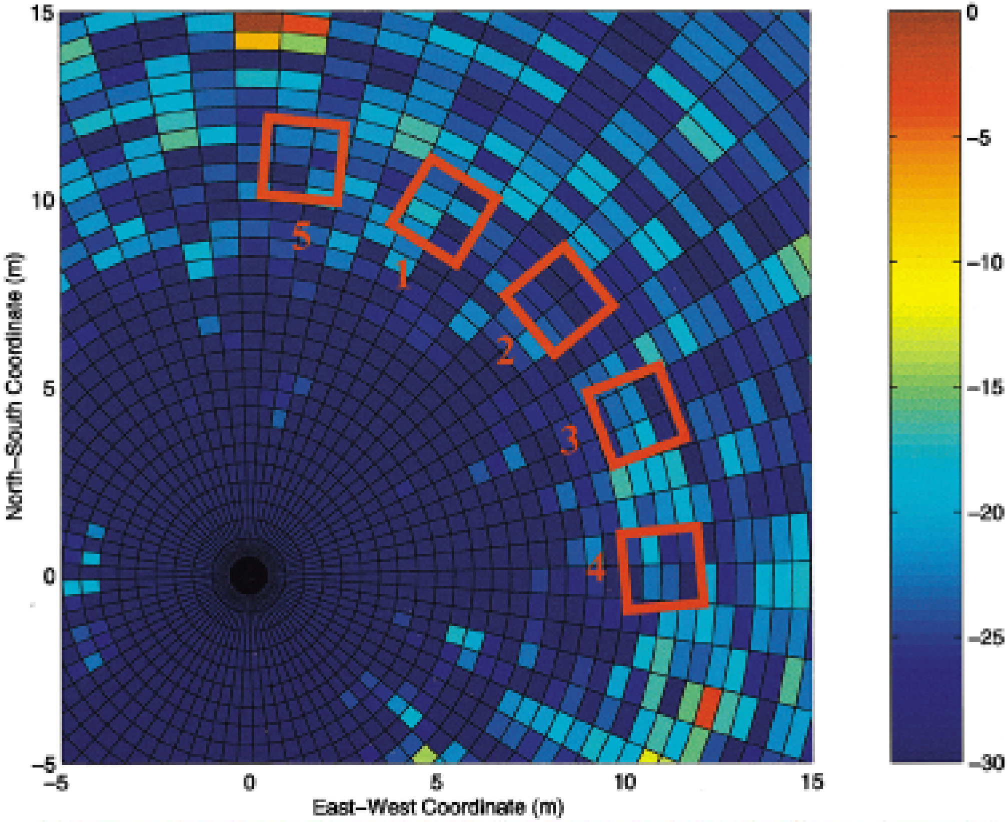

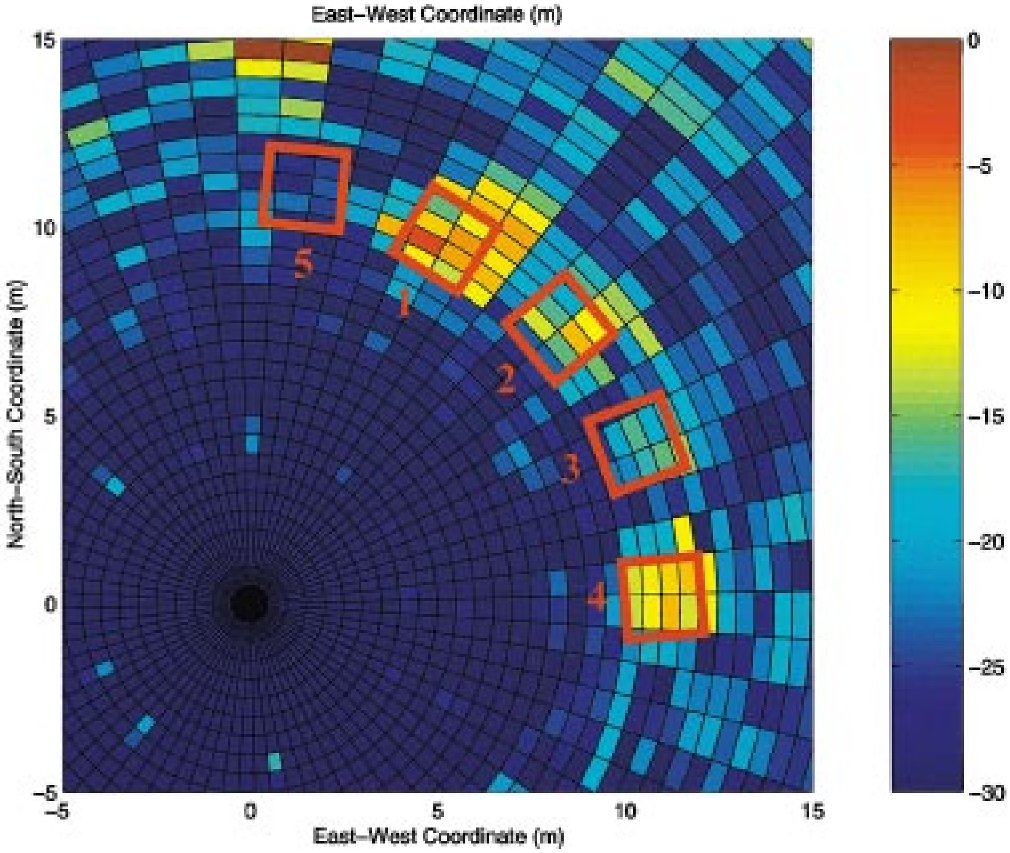

Fig. 7. Backscattered intensity expressed in terms of the Lambert parameter for pixels in the NE quadrant of the acoustic viewing area of the BAMS tower. Each pixel represents 5° of azimuthal angle and 0.5 m of range. Top: scan collected at 0732 on Oct. 22, 1999, (before treatments were done) showing low values of backscattered intensity from all treatment areas. Bottom: scan collected at 1502 on Oct. 27, 1999, (after treatments) showing high backscattered intensity from 4 treatment areas. The highest values of backscattering level are from treatment area #1 with 1000 large glass spheres (35-mm-diameter), followed by treatment area #4 which was raked orthogonal to the BAMS acoustic path, treatment area #2 which contained 281 shells, and treatment area #3 which contained 1000 smaller glass spheres (10-mm-diameter). Treatment area #5 had recently been smoothed and therefore had low values of backscattered intensity.

that allowed the cofferdam to be placed in its desired position, shown in Fig. 4.

The cofferdam is a 1.1 m $\times$ 0.8 m $\times$ 0.6 m sheet metal box open at the top and bottom. Thirty holes had been machined through the side that would be closest to the buried array. A lip was placed along the outside of the cofferdam to indicate when it had been embedded to the correct depth, and four eccentric, pneumatic shakers were temporarily mounted at the top. The cofferdam was placed on the sand using the frame guides. Under the control of divers, pressurized air from the ship was then supplied to the shakers, and the resulting vibration allowed the cofferdam to work its way into the sediment. Periodically, divers shut off air to the shakers and excavated the sand within the cofferdam, taking care to place the excavated sand outside the area of the experiment. Following this procedure, the cofferdam was inserted into the sediment to the desired depth and the sand inside it removed.

The 30 holes in the cofferdam were arranged in five vertical columns with six holes on each column. Divers fastened guides within the cofferdam immediately behind each hole. The guides allowed a hollow rod, holding a B&K 8103 hydrophone at its tip, to be inserted horizontally to the desired length. The rod was then retracted through the guide, leaving the hydrophone in place. This procedure allowed the buried array geometry shown in Fig. 4 to be attained without disturbing the surface above the array. For each of the 5 vertical arrays, the nominal hydrophone depths were 0.06, 0.11, 0.16, 0.21, 0.31, and 0.41 m. The horizontal positions of these arrays occupied the corners and midpoints of two sides of an equilateral triangle of side 0.6 m as shown in Fig. 4.

The position of each buried hydrophone was surveyed relative to the base plates (feet) of the frame legs several times during the experiment. To do this, the frame was unfolded and leveled, and a Y shaped structure was placed on the frame above the buried array. Four ITC 1032's were attached on this structure with their physical centers 0.900$\pm$ 0.005 m above the feet of the frame. The 1032s also had known horizontal separation ($\pm$0.005 m). Each 1032 transmitted 200-ms pulses centered at 30 kHz. The geometry was chosen so that in every case there was a low-loss refracted path from source to buried receiver. From the times of arrival from each 1032 to each buried hydrophone, the positions of the hydrophones were determined with an uncertainty of about $\pm$0.01 m. This was the uncertainty range predicted before the experiment using simulated pulses of sound transmitted through a rough interface [10]. The presumed hydrophone positions were then varied within the $\pm$0.01 m uncertainty range to optimize the resolution seen in speed/angle plots (e.g., see [10, Appendix B]) for geometries where the incident grazing angle was greater than the critical angle. This procedure reduced hydrophone position uncertainty to $\pm$0.005 m and resulted in speed/angle plots that gave good predictions of refracted path grazing angle and sediment sound speed at the highest frequency used (50 kHz). These optimized hydrophone positions were used in the examples shown later in this section.

The four ITC 1032 sources used for the penetration measurements were equally spaced on the STMS tower, with the top one 5 m above the sediment surface and the bottom one 3 m above. Use of four sources allowed data at four grazing angles to be acquired for one tower position. The ITC sources had tuning circuitry to allow operation from 10 to 50 kHz. Transmission data from the tower to the buried array were taken at tower locations defined by the intersections of the 7-, 10-, 15-, and 20-m-radius semicircles with the solid lines radiating outward from the cofferdam in Fig. 4.

A data set for one position of the tower typically included transmissions one second apart at 8 center frequencies from each source. The transmission frequencies were 11, 20, 25, 30, 35, 40, 45, and 50 kHz and each had approximately 10-kHz bandwidth, except the lowest frequency which had 5-kHz bandwidth. For each source and center frequency, several transmissions (normally less than 10, but in some cases up to 100) were sent so that coherent averaging could be used as in the backscattering measurements to reduce the effect of schools of fish sometimes present in the field of view. Thus, for most tower positions there were typically 200–300 transmissions to the buried array. The tower sites at the 7-m range were occupied two times in the course of the experiment, those at 10 m occupied 4 times, and those at 15 m and 20 m occupied once.

Much of the on-board analysis involved examination of data from individual tower locations. As part of that analysis, the complex baseband time series were plotted and then used in constructing speed/angle plots of the penetrating field (e.g., see [10]). Two examples are shown in Fig. 9. In Fig. 9(a), the envelopes of baseband (30-kHz center frequency) time series from a five-transmission average are shown for six of the buried hydrophones (all from one vertical column). The earliest arrival is for the top hydrophone and the arrivals occur in order of hydrophone depth; each is normalized to a maximum envelope value of unity. The geometry is such that the incident grazing angle (38.4°) is greater than the critical angle of about 30°. The corresponding speed/angle plot (using 18 hydrophones) is shown in Fig. 9(b). In the analysis used to generate this display no assumption is made on the value of the sediment sound speed: all values less than 2000 m/s are considered possible. The white curve indicates speed/angle combinations consistent with Snell's law for refraction. The black plus sign marks the highest output from the speed/angle processor, and indicates a propagation angle of 29° and a sediment sound speed of 1760 m/s, values fully consistent with refraction at a flat water-sediment interface. The sediment speed is also in the range found by other researchers during SAX99 (see [1]). Fig. 9(c) and (d) is the time series and a speed/angle plot for a case with the incident grazing angle (18.2°) below the critical angle. The time series in Fig. 9(c) are much closer together, more complicated, and not in the same order as Fig. 9(a). In addition, the highest output of the processor is not near the Snell's law curve. These measurements of penetration both above and below the critical angle will be compared to the predictions of different penetration hypotheses and will be used in examining spatial and temporal coherence issues.

In the last few days of the experiment, the surface of the sediment above the buried array was altered and then penetration data acquired. Alterations included smoothing the surface and the creation of small-scale ripples similar to the ripples used in backscattering measurements, except the ripple wavelength

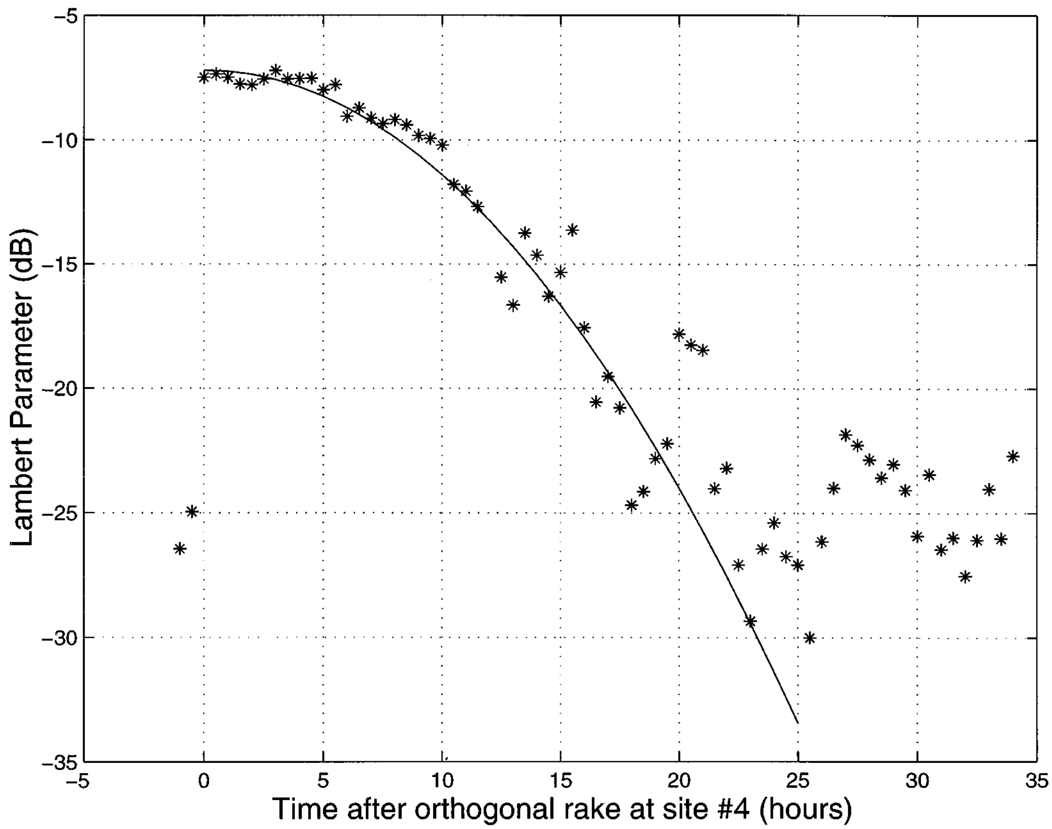

Fig. 8. Decay of 40-kHz backscattered intensity (averaged over 5 pixels in the center of treatment site #4) after the sediment surface was raked orthogonal to the acoustic path from BAMS. The backscattered intensity is expressed in term of the Lambert parameter. The solid line is a curve fit to the data and expresses the Lambert parameter (in decibels) as $-7.2 - 0.042t^2$ where t is the time since treatment expressed in hours.

was the same as the acoustic wavelength at 40 kHz. Stereo photographs were taken after each manipulation of the sediment was carried out and then a set of acoustic data was acquired. These measurements will be used as further checks on acoustic penetration hypotheses.

D. Attenuation Measurements

Accurate sediment attenuation measurements over a broad range of frequencies may lead to important constraints on acoustic propagation models for sediments. In preparation for SAX99, broad-band tuning circuits were built so that the usable source frequency band for the ITC 6148s in the diver deployed attenuation array is from 80 to 300 kHz. This frequency range overlaps the frequency ranges of the NRL attenuation measurements (10–100 kHz) and the APL-UW acoustic tomography (130–180 kHz) and penetration (10–50 kHz) measurements that also produce attenuation data. These overlaps will allow consistency checks of results.

The attenuation array consists of two transmitters and two receivers giving four separate paths for which measurements were taken. Both transmitters and receivers are 6148s (with an active element about 0.7 cm in diameter, and with a sensor diameter including waterproof jacket of a little less than 1 cm) and are mounted at the ends of separate legs of a rigid frame. The electronics and data acquisition systems are packaged in a pressurized housing, which is also mounted on the frame. The four elements are almost aligned in a straight line, but they are offset enough from a line so that none of the ray paths is obstructed by the inner legs. The two transmitters are on the outer legs with the receivers on the inner legs. We designate ray path length P_{lm} as the distance from transmitter l to receiver m where $l, m = 1$ or 2. There are a total of four rays paths with path lengths $P_{11} = 22.9$ cm, $P_{12} = 44.1$ cm, $P_{21} = 43.5$ cm, and $P_{22} = 22.2$ cm. During the experiment, the attenuation array was first set on the seafloor with all 6148s in the water and a set of calibration data was taken. Then divers pushed the elements into the sediment (in most cases to a depth of about 10 cm), and a set of data was taken. A data set consisted of 48 transmissions of 100-ms pulses from each source to each receiver. Each transmitted pulse had about 10-kHz bandwidth and 12 center frequencies were used over the 80-300-kHz range in steps of 20 kHz. This cycle of 12 center frequencies was repeated four times to get the 48 transmissions quoted above. During SAX99, 42 sets of in-sediment attenuation data were taken.

Data taken at 100 kHz at 11 of the 42 measurement sites are shown in Fig. 10. The sediment absorption coefficient is estimated by comparing the integral of the square of the waveform envelope with those of the calibration data, assuming that the absorption coefficient of water is negligible. For each of the four paths, estimates of the absorption coefficient were obtained for each of the 11 sites and are shown in the figure. The average absorption coefficient for the 11 sites is also given for each path: α_{11} was obtained using path length P_{11}, and so on. The average over all four paths is 30.5 dB/m, or, equivalently, 0.305 dB/m/kHz at 100 kHz. The large fluctuations observed in Fig. 10

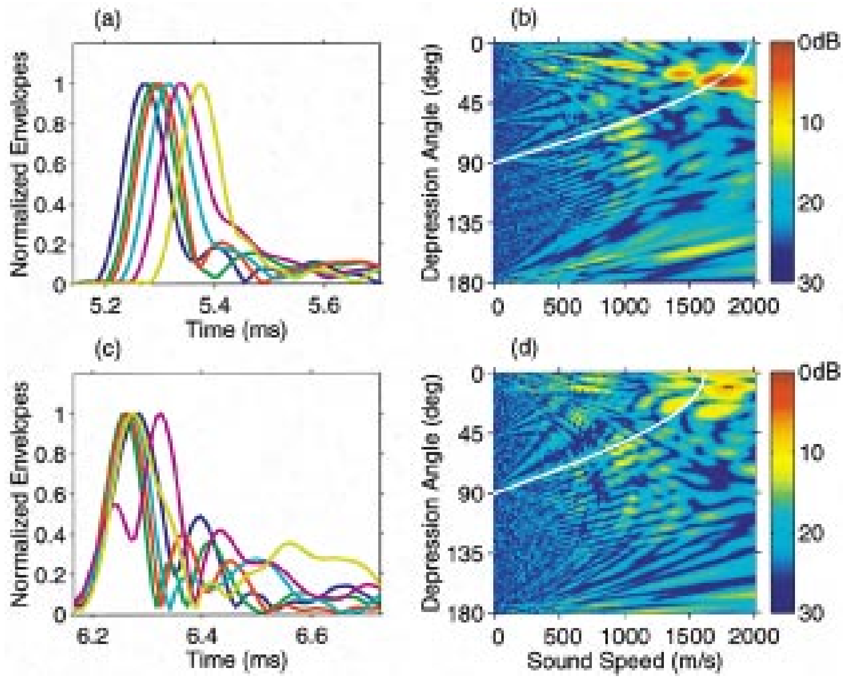

Fig. 9. Two examples from acoustic penetration experiments. For the first example [(a),(b)], the incident grazing angle of $38.4°$ is greater than the critical angle of about $30°$. Baseband (30-kHz center frequency) time series from a five-transmission average are shown in (a) for transmissions from the mobile tower to six of the buried hydrophones (all from one vertical column). The earliest arrival is for the top hydrophone and the arrivals occur in order of hydrophone depth. The corresponding speed/angle plot (using 18 hydrophones) is shown in (b). The white curve indicates speed/angle combinations consistent with Snell's law. The black plus sign marks the highest output from the speed/angle processor and corresponds to a propagation angle of $29°$ and the sediment sound speed 1760 m/s. Time series and a speed/angle plot for an example with the incident grazing angle $(18.1°)$ less than the critical angle are shown in (c) and (d), respectively. The plus sign in (d) corresponds to a propagation angle of $11°$ and a sediment sound speed of 1800 m/s.

probably indicate that scattering is significantly affecting the absorption estimates. A challenge in the data interpretation will be to assess the relative importance (as a function of frequency) of absorption and scattering in attenuating an acoustic wave in sediment.

IV. ARL:UT Experiments During SAX99

The participation of the Applied Research Laboratories of the University of Texas at Austin (ARL:UT) was directed toward determining the underlying physical processes in the penetration of sound into sandy ocean sediments, particularly at shallow grazing angles, and the scattering of sound from the sediment. Recent work at ARL:UT has examined the possible role of the poro-elastic solid (Biot) model of sediments in explaining acoustic penetration at subcritical grazing angles [2], but processes that combine poro-elastic and scattering effects are also being considered. In particular, these considerations have suggested that, while the Biot slow wave penetration mechanism is applicable to a uniform sediment with a flat surface, it may be enhanced by surface roughness and volume heterogeneity through energy conversion between the slow and fast waves.

The ARL:UT experiments were designed to distinguish between the penetration hypotheses based on: 1) the poro-elastic mechanism and 2) scattering from surface and/or volume heterogeneity of a sediment represented as a fluid. To test these hypotheses, a number of new measurement methods were developed. These methods were designed to eliminate the shortcomings in previous studies and provide the necessary discrimination between the candidate hypotheses. They were realized in an operation involving a mobile sound source carried on a remotely operated vehicle (ROV) in combination with tilted, rigidly supported, buried acoustic line arrays, illustrated in Fig. 11.

Tilted buried line arrays, on rigid supports, were used instead of the vertical buried line arrays of past experiments. With vertical arrays, it has been argued that scattering artifacts at the water–sand interface could have been generated at the insertion point. Such an artifact could have the appearance of a slow refracted wave. With the tilted geometry, the sediment directly above the acoustic sensing elements is undisturbed, eliminating the possibility of scattering artifacts from within a cone of angles about the vertical. The sensing elements were acoustically isolated from the support structure by sound absorbing materials. Scattering artifacts at the point of entry would be greatly attenuated due to the obliqueness of the path and may be rejected by time gating. The improved positioning accuracy due to rigid supports allows coherent processing up to 200 kHz, which is an essential requirement for distinguishing between a refracted wave, which tends to be coherent, and scattered sound energy which is incoherent. Two arrays were deployed, one facing $60°$ relative to magnetic north and the other at $240°$.

Broad-band signals, made possible by new transducer materials, were used in order to detect frequency-dependent trends in both penetration and scattering to provide important clues to the underlying physical mechanisms. Of particular interest are the attenuation, transmission and scattering coefficients as functions of frequency. Existing empirical models [32] assumed that attenuation is linearly proportional to frequency, but older [33] and more recent [34] laboratory experiments show significant

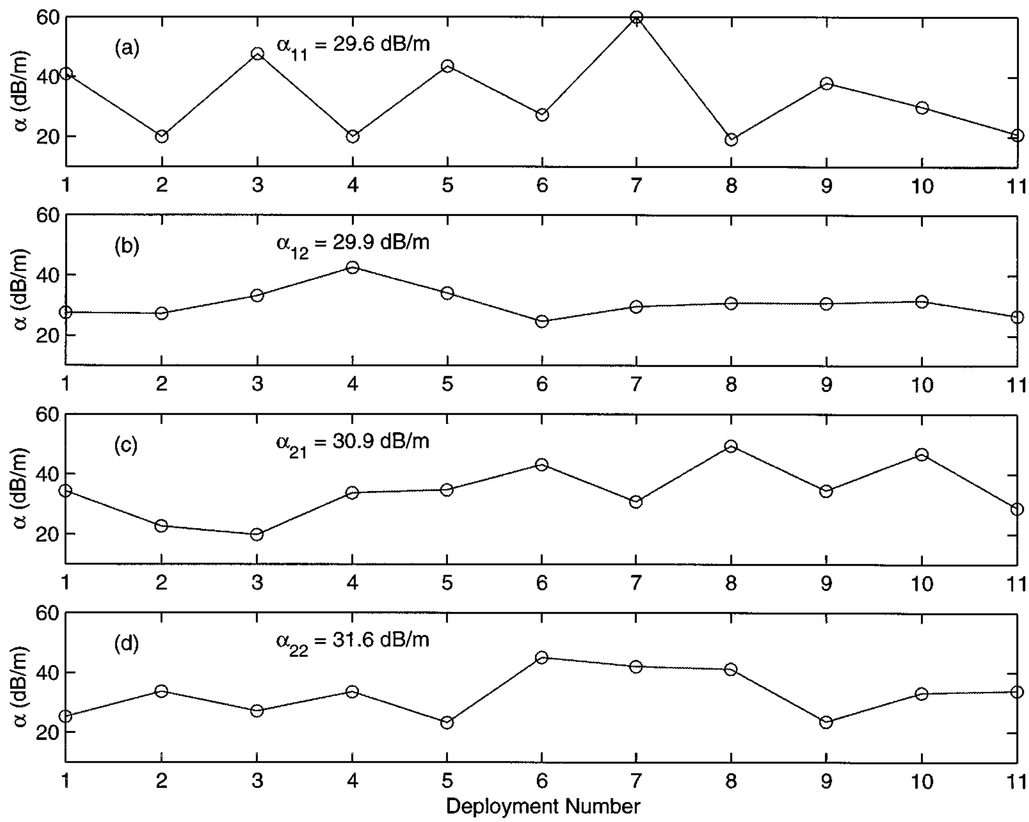

Fig. 10. Data acquired at 100 kHz for 11 deployments of the APL-UW attenuation array. The four panels are for the four acoustic paths realized on the array. Each data point plotted in a panel is an estimated absorption value based on a single deployment; the values quoted are the 11-deployment averages for each path. The path lengths for each path are given in the text.

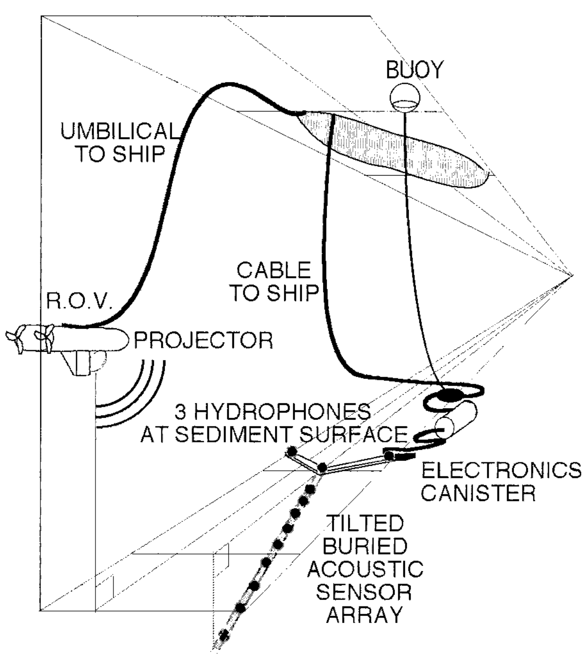

Fig. 11. Experiment layout showing ARL:UT buried acoustic receiving array and sound projector on an ROV.

deviations. On a practical level, broad-band signals allow sparse arrays to be used in the estimation of direction and speed of coherent waves, and phase coherence across a broad band is a good indicator of a refracted wave, as opposed to a scattered wave.

Using an ROV as the platform for the sound source and backscatter receiver provided several advantages. The mobility provided by an ROV allows the buried array to be ensonified over a continuous range of grazing and azimuth angles. It is possible to observe the dependence of bottom backscattering strength on height above bottom, which is an indicator of single or multiple scattering. Such a dependence was first observed in a recent experiment [35]. It is also possible to obtain an ensemble of backscattering measurements from a large area, as a function of grazing angle and bearing, providing enough independent data points to construct a detailed frequency distribution curve. The frequency dependence of the Q-factor of the scattered signal is another independent indicator of single or multiple scattering; multiple scattering processes are known to cause an increase in Q-factor with frequency [36]. A complication associated with using a moving sound source is determining the position of the sound source at each ping. This was done by triangulation and time of flight measurements using three hydrophones on the support structure at the sediment surface.

The buried arrays were made of 1–3 composite receiving elements slotted into a stainless steel tubular structure. The tip of the buried section was designed to be 0.77 m below the surface of the sediment, as shown in Fig. 12. The receivers were numbered 4 through 15, of which 4, 5 and 6 were on the surface of the sediment. Examples of the raw signals from the buried section of the array are shown in Fig. 13. In this case, the sound projector was at a range of approximately 6 m, and at a grazing

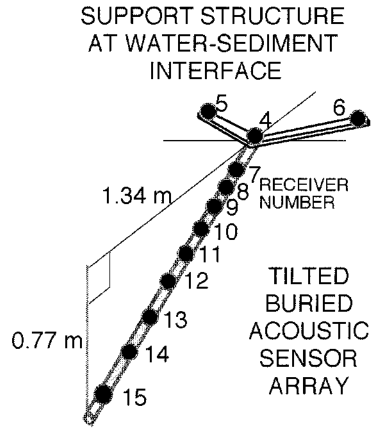

Fig. 12. The ARL:UT buried array.

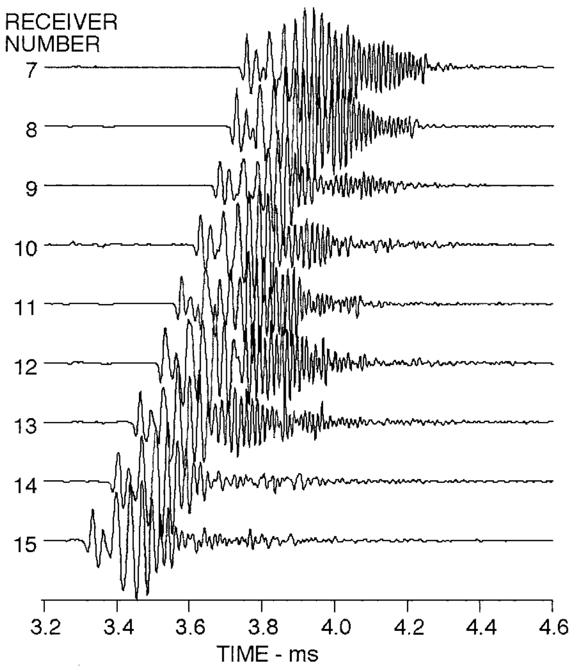

Fig. 13. Example of raw acoustic signal from the buried receivers.

angle of approximately $30°$, with reference to receiver number 4. The signal was a chirp from 10 to 100 kHz. It is clear that the high-frequency components were unable to reach the deepest receivers. After pulse compression with a replica of the transmitted pulse, all of the signals were transformed into a band-limited impulse, indicative of a coherent wave front, as shown in Fig. 14.

The task ahead is to analyze all the signals, particularly those at shallow grazing angles. New analysis algorithms will be applied to explore the nature of the sound field in the sediment and to determine if it is refracted or scattered. Backscattered signals will also be analyzed to determine the order of the scattering process, according to the objectives and approaches outlined above. The acoustic results will be used in conjunction with the environmental characterization of the sediment provided [1] to develop a better understanding of the relationships between geophysical properties of the sediment and its acoustic behavior.

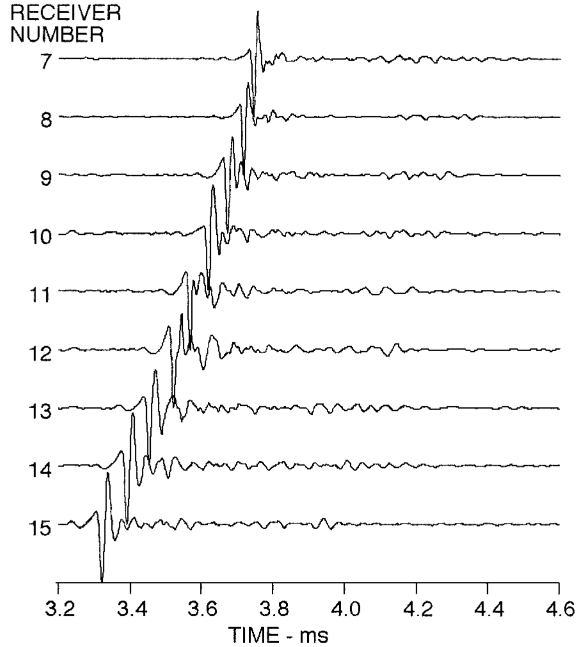

Fig. 14. Example of pulse compressed acoustic signal.

V. BAE SYSTEMS Participation in SAX99

BAE SYSTEMS (formerly Tracor) scientists deployed a number of acoustical sensors during SAX99. The principal goal of this effort was to monitor the flux of benthic organisms into and out of the bottom to examine the hypothesis that bioturbation would affect the acoustic properties of the bottom as these animals dug burrows in the sediments as refuges during the day. The systems deployed for this purpose are described in the companion paper [1].

A set of acoustic sensors was deployed for the purpose of measuring bottom scattering properties at high and low frequencies. These sensors, mounted on a tower placed on the bottom about 40 m south of the APL-UW BAMS system, consisted of a high-frequency echosounder (TAPS-8) and a video camera, both on a remotely controlled pan/tilt mechanism, and a low-frequency acoustic system consisting of a line-in-cone source transducer and a line array receiver. [TAPS denotes Tracor Acoustic Profiling System.] All systems were cabled to the R/V Seward Johnson and operated from a van on the forecastle. The TAPS-8 was controlled by a computer that could execute a pre-recorded script at selected times, collecting data at a set of programmed pan and tilt angles and storing the data. Data were transmitted via a spread spectrum RF link to a shore lab for near-real-time processing.

The TAPS-8, located 3.5 m above the bottom, was used to measure bottom backscattering at eight discrete frequencies: 104 kHz, 165 kHz, 265 kHz, 420 kHz, 700 kHz, 1.1 MHz, 1.85 MHz, and 3 MHz. The transducers were all circular-piston elements chosen to provide beam widths of approximately $10°$. Data were normally collected at $5°$ increments of pan and at $5°$ increments of depression angle from $15–30°$. TAPS-8 was adapted from a device designed to measure volume scattering strengths of zooplankton and only recorded echo intensities.

Thus, the data consisted of averaged echo intensities over a selected number of pings (usually 24) in fixed range bins at 12.5 cm intervals. Pulse lengths were fixed at $336\ \mu s$.

A typical image obtained at 420 kHz during a high-resolution (1° azimuthal steps) bottom scan is shown in Fig. 15. Bottom backscattered intensities have been converted to Lambert's parameter as described in Section III-B. The echo to the left of center at approximately 14 m range is from a 61-cm metal sphere target sitting on the bottom. Elsewhere, considerable structure is evident, although it is exaggerated in angle because of the 10° beamwidths. The cause of this structure is not entirely certain; it is possible that interference from fish could be producing some of the fluctuations. Averaging over space and time should help reduce the contributions of the (relatively rare) fish to tolerable levels in the computation of the bottom backscattering strengths. It is anticipated that this data set will provide a useful extension in frequency to the body of measured bottom backscattering strengths for sandy bottoms.

The low-frequency system was included primarily to provide a set of scattering data from buried and proud targets for further analysis by R. Lim of CSS in his studies of sound scattering at subcritical angles of incidence [37], [38]. Measurements of bottom scattering strengths at frequencies below those of the other participants were also desired.

This system was attached to the tower at 2.2 m above the bottom, aimed in a fixed direction, and the tower was installed so that this system pointed directly at a buried 61 cm diameter metal sphere at a range of 9.6 m; the grazing angle of 13° was well below the critical angle of about 30°. The source transducer was a line-in-cone design with an aperture of 38 cm, driven by a 1-kW power amplifier. Useful outputs were obtained from 2 to 24 kHz. Transmitted signals consisted of short (1.5 and 3 ms) CW pulses and wideband signals (composed of 13-bit Barker codes impressed as 180° phase shifts on CW carriers), both signal types being generated at 2 kHz intervals.

Echoes were received either though the source transducer, via a diode T/R switch at the power amplifier, or through a 1.5 m horizontal line array specially fabricated for this experiment. The line array was composed of five separately wired sections that could be electrically combined to adjust the directivity to be sensibly constant (approximately 10° in the horizontal and essentially omnidirectional in the vertical) over frequency. A pre-amplifier and relay unit mounted near the array selected the array segments and drove signals up the cable to the ship.

The low-frequency system was also controlled by the shipboard computer but the data collection program had to be manually selected. This was done for safety reasons due to the heavy diving schedule and also to allow us to ensure that there were no marine mammals in the vicinity prior to active operations. Data were collected according to pre-recorded scripts specifying the signal type (CW or coded), duration, center frequency, and other parameters controlling the received signal path. Echoes were digitized at 160 kHz with a 16-bit resolution analog to digital converter; signals were stored as raw samples, no averaging or processing was done at that time. Groups of 20 pings at each frequency were recorded in each set. Pings were generated at about 1-s intervals, thus measures of echo properties are short-term measures.

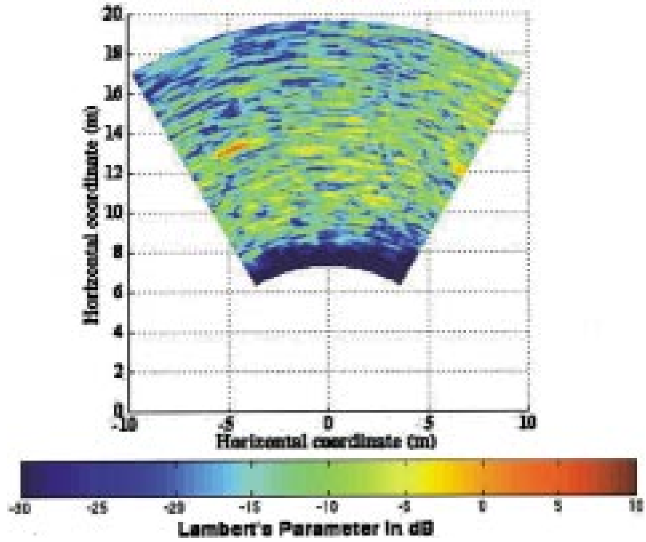

Fig. 15. Image of bottom backscattered intensity converted to Lambert's parameter taken by the TAPS-8 at 420 kHz and a depression angle of 15°. Horizontal range resolution is approximately 12.5 cm. Azimuthal steps were 1° although beamwidths were approximately 10°. The strong scattering to the left of center at a range of 14 m is due to a target sphere laying on the seabed.

The video camera was not able to produce high quality images of the bottom, due in part to its distance off the bottom (3.5 m) and the generally turbid conditions. The camera did prove useful in observations of the fishes attracted to the tower, however. At times, the bottom was completely obscured by schools of bait fish (hard-tailed jack) and predators (*cobia* and other species) surrounding the top of the tower. No reactions from the fish to acoustic transmissions were observed for either the high- or low-frequency system.

For most of the experimental period, the sphere target remained buried just below the surface. On the last day of the experiment, divers extracted the sphere from the bottom and laid it on the seabed at a range of about 14 m so that we could collect a set of data in that configuration. Fig. 16 shows a typical result from the low-frequency system at 6 kHz. The echo from the proud sphere target is evident at a range of about 15 m. We computed a measure of echo variability (the intensity variance divided by the mean-squared intensity) as a way to discriminate deterministic from fluctuating echoes. As the lower panel in Fig. 16 shows, there are regions in range where the echoes are dominated by the (short-term) fluctuating component; presumably these are echoes from the abundant fish schools in the area. It remains to be seen if further averaging can reduce the fluctuating component to sufficiently low levels to allow us to extract bottom scattering strengths from these data.

VI. CSS Participation in SAX99

A. Synthetic Aperture Sonar

A synthetic aperture sonar (SAS) system operated by Coastal Systems Station (CSS) was used during SAX99. Synthetic aperture sonar is a type of side-scan sonar that uses coherent processing of multiple ping data to effectively create a much larger array length, allowing high resolution images to be generated [39], [40].

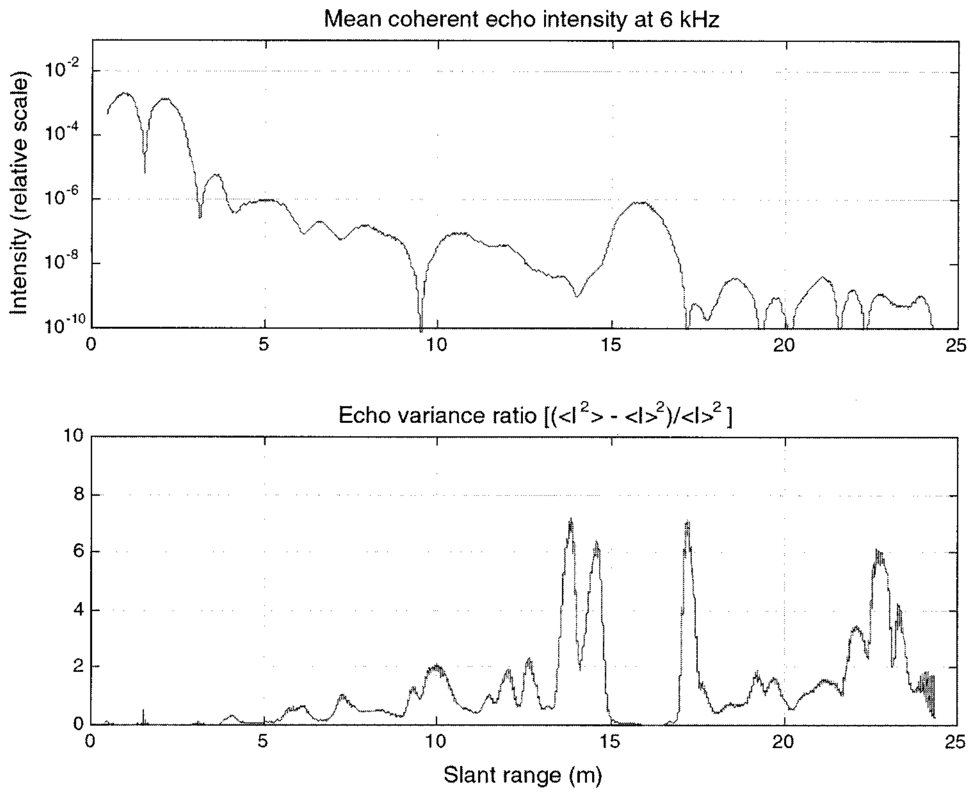

Fig. 16. Typical echo sequence from the low frequency system. Top: intensity of the mean (coherent average of 20 complex waveforms) echo versus slant range. The sphere target is evident at a range of 15 m. Bottom: the ratio of the echo intensity variance to the mean-squared echo intensity for the 20-ping echo sequence. This measure, adapted from use in volume-scattering work, serves to discriminate regions of deterministic signals (such as the sphere echo, where this ratio approaches zero) from regions dominated by fluctuating echoes. For example, echoes arising from volume scattering involving a large number of scatterers would have a variance ratio of unity.

The SAS system used in this experiment is housed in a 53 cm diameter towbody. It has both high-frequency (180 kHz) and low-frequency (20 kHz) arrays on the port and starboard sides. The high-frequency array has 11 elements and has demonstrated a 2.5 cm resolution capability. The low-frequency array has 14 elements and has approximately 7.5 cm resolution. This array has some capability of penetrating through the sand sediment to detect buried objects. A nominal detection range for the system is 40 meters at a tow speed of 8 knots with the height of the towbody at 4.0 ± 0.5 m above the bottom.

An example of an SAS high-frequency image made at the SAX99 site is shown in Fig. 17. A cylindrical target lying on the surface and the rippled seabed are clearly evident. The sound is incident from the left and the acoustic shadow to the right of the target can also be clearly seen. The total size of the image is 9 m by 9 m, and the ripple wavelength is about 50 cm, as mentioned previously. The cylindrical target is 1.5 m in length and about 27 cm in diameter.

SAS measurements were also made in the target field near Panama City (Fig. 1), and ripple was present on the seafloor similar to the ripple at the SAX99 site. The target field contained two buried and two partially buried cylindrical targets. The two partially buried targets were easily seen by both the high-frequency and low-frequency arrays. One of the buried targets was under about 15 cm of sand and had been only recently buried; it was detected with both the high-frequency and low-frequency arrays.

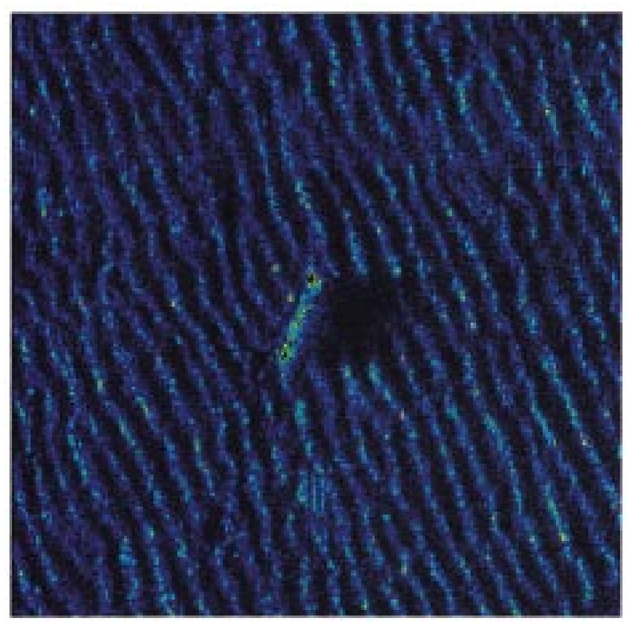

Fig. 17. High-frequency (180-kHz) SAS image of cylindrical target.

The other buried target had been in place for about six months and was covered by approximately 50 cm of sand. The low-frequency image of this target is shown in Fig. 2; the target is near the center of the 9 m by 9 m image. (The

TABLE III
TARGETS USED IN CSS MEASUREMENTS AT THE SAX99 SITE.

Target Line (Bearing)	Target #	Target Type	Cylinder Aspect Angle	Angle R-R MRA Makes With Horizontal.	Range (m)/ Slant Range (m)	Grazing Angle
270°	1	Cylinder	0°	—	16.3/16.6	10°
270°	2	Cylinder	0°	—	7.7/8.3	20°
180°	3	Cylinder	20°	—	18.3/18.5	9°
90°	4	20.3-cm R-R	—	22°	4.5/5.3	35°
90°	5	20.3-cm R-R	—	0°	7.9/8.4	20°
90°	6	30.5-cm R-R	—	0°	16.7/17	10°
148°	7	20.3-cm R-R	—	45°	7.9/8.4	20°
148°	8	30.5-cm R-R	—	45°	17.1/17.3	10°
210°	9	20.3-cm R-R	—	80°	7.9/8.4	20°
210°	10	20.3-cm R-R	—	80°	16.5/16.7	10°

Note: (a) R-R is an abbreviation for retro-reflector.
(b) The cylindrical target's aspect angle is defined as the angle made by the normal to the length of the cylinder with respect to the direction of the incident acoustic beam.

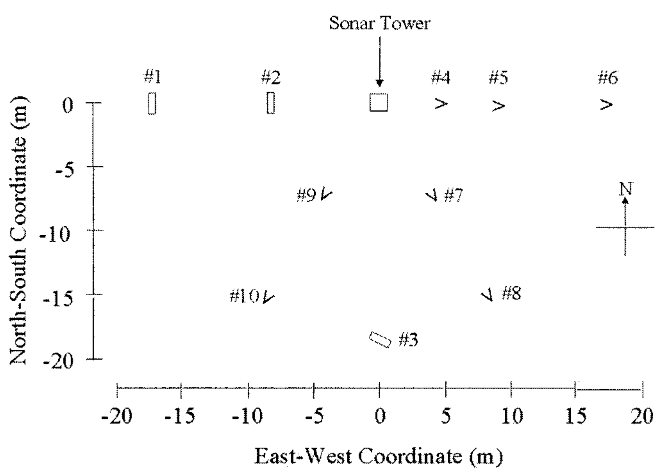

Fig. 18. CSS target field at SAX99 site.

feature in the lower left is a marker left by the divers.) The 20 kHz sound was incident from the left at a range of 50 m from the cylindrical target, which has a length of 1.9 m and a diameter of 47 cm. The range combined with the height of the towbody leads to an incident grazing angle at the bottom of 4° to 5°, far below the critical angle of 30°. The peak target return is about 22 dB above the background level, which is due to backscattering from the seafloor. The target has a broadside aspect with respect to the direction of the SAS; this aspect is favorable and may contribute to the somewhat unexpected detection at this depth. On the other hand, the existence of two prominent features may indicate that the scattering is from the corners at the two ends of the cylinder.

Because of the high resolution of the SAS system, the background scatter from the seafloor occurs from a very small area and is thus relatively low; this is a significant advantage over conventional sonars for buried target detection. A subcritical detection is most likely the result of acoustic penetration due to scatter from ripple as discussed in Section III-C. Further analysis will be needed to fully understand the origin of this detection.

B. Buried Target Sonar System

CSS investigators carried out a separate study during SAX99 to explore the ability of conventional sonars to detect buried targets. While SAS techniques have a clear advantage over conventional sonars at longer ranges, use of conventional sonars could still be a useful approach at short range where SAS systems may not be as practical. At sufficiently short range, the background scatter from the sediment surface will occur from a very small area for a conventional system, and thus the potential for subcritical target detections should be present. The SAX99 measurements were based on an acoustic lens sonar system [41] under development at CSS, and the main goal was to assess the performance of this system against buried targets.

1) Measurement Setup: A target field consisting of ten bottom targets was deployed by divers (Fig. 18), and acoustic measurements were made from a 3-m-high sonar tower. Targets 1–3 were cylinders 1.5 m in length and about 27 cm in diameter. Targets 1 and 2 were buried by divers using water-jetting methods; target 3 was placed on the bottom. Positions of all targets relative to the tower are shown in Fig. 18 and listed in Table III.

Targets 4–10 were calibrated conical retro-reflectors 20.3 cm or 30.5 cm in diameter and have relatively constant target strength over a wide aspect angle. The in-water target strength of the 20.3-cm (30.5 cm) diameter retro-reflectors ranges from −9 dB (–5 dB) at 40 kHz to +7.9 dB (+11.8 dB) at 100 kHz. These targets were hand-buried by divers just below the water–sediment interface with the aid of a jig that helped to adjust the burial depth and set the vertical component of the maximum response axis (MRA) of each retro-reflector. The horizontal component of the MRA for each retro-reflector was directed toward the sonar tower. Table III lists the pertinent information for all of targets used in the measurements. Note that, with the exception of target 4, all targets were below the critical angle of about 30°.

Divers periodically inspected the target field. They noted that the ridges on the bottom sediment ran at a compass heading of approximately 35°. In addition, they estimated (by sight) that the rippled structure was about 70 cm crest-to-crest with a peak-to-trough height of almost 4 cm and a width of approximately 8 cm (estimated at half of the peak-to-trough height). They also noted that there were little to no bottom currents during the measurement period. During the burial process of targets 1 and 2, they reported that the air could not be completely bled out of the water-jet apparatus, and thus some air was introduced into the surrounding sediment. They also observed that the burial process introduced a faint scar in the bottom sediment over target 1. After burying each retro-reflector, they restored the original ridge structure over each of these targets by sculpting ridges to closely mimic the area prior to the burial. In addition, they recorded that target 1 was completely buried at least 2 cm deep, target 2 was partially exposed (one end was fully buried while the other was 1.3 cm above the sediment), target 3 was proud of (i.e., on top of) the bottom, and each retro-reflector was completely buried by at least 6 mm of sediment.

The sonar tower was positioned on the bottom approximately 190 m south of the R/V Seward Johnson, and the sonars were about 3 m above the bottom. The tower supported three acoustic sensors and scanning (horizontal pan and vertical tilt) motors such that the acoustic sensors had an almost 360° (180°) rotational (tilt) capability. In addition, a pendulum tilt sensor was employed to monitor the inclination angle of the various acoustic sensor MRA's.

The three acoustic sensors on the tower were an acoustic lens subsystem (which will be referred to as the lens), a line array, and a NUWC-USRD (Naval Undersea Warfare Center Underwater Sound Reference Detachment) type F33 transducer (which will be referred to as the F33). The lens has an aperture 25 cm in diameter and is partially populated using acoustic elements that operate between 30 and 60 kHz. The lens transmits a conical beam that has a one-way 3 dB-down beamwidth of 8.5° at 50 kHz. The line array has an aperture measuring 67 cm by 3.5 cm, an operational band from 40 to 60 kHz, and is oriented such that its narrow beam is in the horizontal plane. At 50 kHz, it has one-way 3-dB down horizontal and vertical beam widths of 2.3° and 46°, respectively. The F33 is operated at 20 kHz. The lens and the line array were used to obtain buried target detection data while the F33 was employed for bistatic acoustic data collection. Cables for the various sensors and for powering/controlling the motors on the sonar tower ran along the bottom sediment from the sonar tower to instrumentation located aboard the R/V Seward Johnson.

Transmitted signals for target detection included 0.1-ms sinusoidal pulses as well as 1.0 ms linear frequency modulated (LFM) pulses; both pulse types had a cosine taper on the leading and trailing edge to minimize ringing in the waveforms generated by the source. Data were acquired by either horizontally rotating the sonars in 0.5° increments at a constant tilt angle, or by vertically tilting the sonars in 1.0° increments at a constant bearing (pan) angle. In all instances, the data obtain at each angle represent the results of a 10-ping coherent average.

2) Results: Data were acquired under calm conditions, with sea states less than 2. The data were analyzed using relative backscatter image scans in which the sonar tower has coordinates (0,0). Figs. 19 and 20 illustrate image scans acquired with the line array using a 40-kHz, 0.1-ms sinusoidal pulse, with the tilt angle of the line array's MRA at 20°. The displayed data correspond to ping times between 6.5 and 14.5 ms and the data shown in these figures were acquired within 10 h of the dive in which divers recorded that the retro-reflectors were buried by at least 6 mm of sediment. Backscattered returns from targets 4 [coordinates (5.3, 0)] and 5 [coordinates (8.4, 0)] are easily seen in Fig. 19; the signal-to-noise ratio (SNR) is over 15 dB for target 4 and about 4 dB for target 5. Several returns are observed in Fig. 20. A return appears at coordinates $(4.6, -7)$, the expected position of target 7. The other returns appearing in the Fig. 20 are due to backscatter from the bottom sediment; such returns do not appear in Fig. 19 due to use of a different amplitude scale.

Fig. 21 illustrates an image scan obtained with the lens. The transmitted signal is a 1.0 ms, 60 to 30 kHz LFM pulse. This figure refers to the data collected by vertically rotating the sensor from a grazing angle of 7° to 27°. The sensor is directed toward the targets located west (270° bearing) of the sonar tower. This image scan is obtained by cross-correlating the backscattered signals with the LFM pulse input to the power amplifier. A correlated backscattered return from target 2 appears at coordinates $(-7.9, -3)$; the SNR is about 5 dB. A second, low amplitude correlated return is also seen at coordinates $(-16.3, -3)$ which is the location of target 1. This second return may be due to scattering from either the buried target, the faint scar in the bottom sediment over target 1, or air in the sediment that was introduced by the water-jet.

Preliminary SAX99 results show that under some conditions buried targets can be detected at short range by conventional sonars at subcritical grazing angles. Future analysis will include investigating the degree to which the backscatter signal is correlated with the incidence pulse and determining the coherence of the signals transmitted into the sediment.

VII. Concluding Remarks

Clearly, much remains to be done in analyzing the acoustics data gathered during SAX99. In fact, that process had barely begun at the time this paper was prepared. Completing the processing of the extensive acoustics data sets should add much to our understanding of high-frequency sediment acoustics. However, the most significant and enduring results to come out this effort will undoubtedly await our utilization of the environmental characterizations summarized in Richardson *et al.* [1] in order to understand the acoustics results in terms of the sediment physical and biological descriptions.

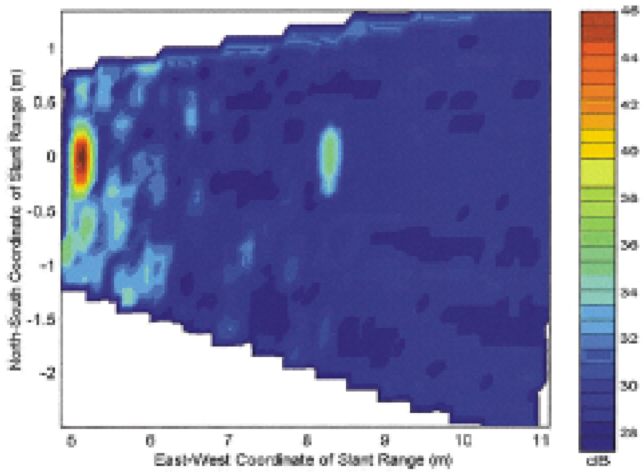

Fig. 19. Image scan corresponding to bearing angles ranging from $83°$ to $104°$.

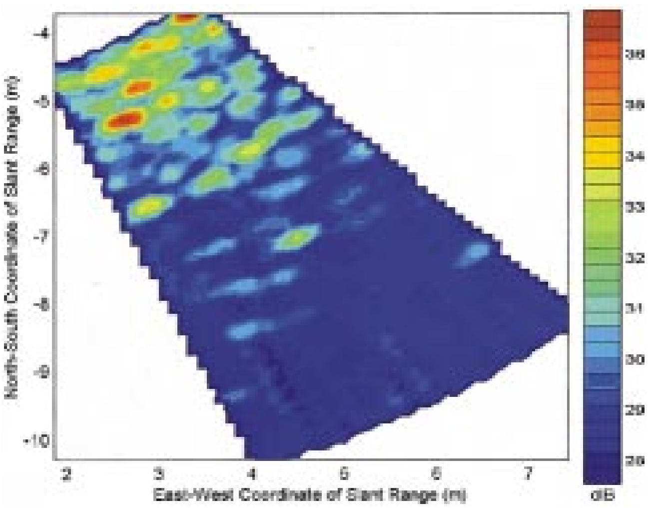

Fig. 20. Image scan corresponding to bearing angles ranging from $138°$ to $159°$

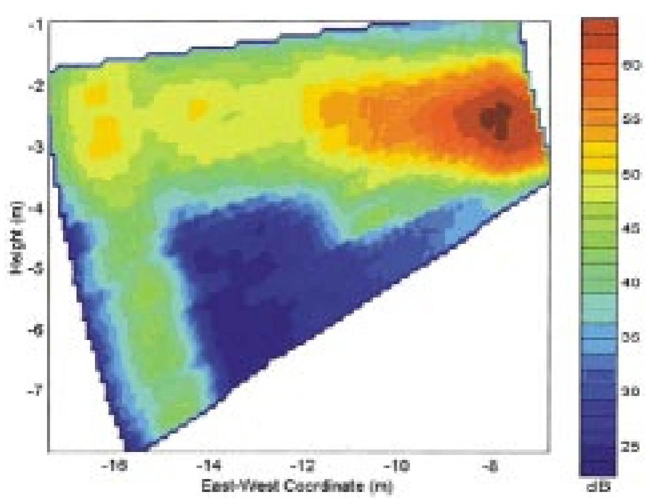

Fig. 21. Image scan obtained with the lens.

ACKNOWLEDGMENT

APL-UW engineer L. Olson was responsible for the deployment and recovery of equipment for many of the experiments described both here and in [1]. He also acted as lead diver during SAX99. His organization, dedication to duty, and attention to detail ensured both success and safety. APL-UW dive team members E. Boget, P. Aguilar, T. Lehman, and M. Ohmart each carried out multiple logistics duties in addition to their diving responsibilities. K. Bader (APL-UW) was the on-shore point of contact. She made the transition from airport to ship seamless for SAX99 researchers and acquired their essential but overlooked supplies. Together, APL-UW engineers V. Miller, R. Light, L. Olson, and M. Kenney designed, built, tested, and operated the APL-UW equipment used in SAX99. The deployment and recovery of the ARL:UT underwater units, sediment coring, photo-documentation and the piloting of the ROV was by the ARL:UT dive team under the leadership of J. Piper. D. E. Smith, of ARL:UT and Los Alamos, gave valuable assistance in the design of the experiments and in the data collection. The buried receivers and sound projector were made by B. McCurley, K. Kirksey, and H. Ma, ARL:UT. The data collection system was designed by K. Lent and N. Crow, and constructed by the staff and students of the Engineering Acoustics Division, ARL:UT. The excellent logistical support provided by CSS personnel was greatly appreciated. The entire experimental effort benefited from excellent support of the captains and crews of the R/V Seward Johnson (Harbor Branch Foundation, Fort Pierce FL) and the R/V Pelican (LUMCOM, Cocodrie LA).

REFERENCES

[1] M. D. Richardson, K. B. Briggs, D. L. Bibee, P. A. Jumars, W. B. Sawyer, D. B. Albert, R. H. Bennett, T. K. Berger, M. J. Buckingham, N. P. Chotiros, P. H. Dahl, N. T. Dewitt, P. Fleischer, R. Flood, C. F. Greenlaw, D. V. Holliday, M. H. Hulbert, M. P. Hutnak, P. D. Jackson, J. S. Jaffe, H. P. Johnson, D. L. Lavoie, A. P. Lyons, C. S. Martens, D. E. McGehee, K. D. Moore, T. H. Orsi, J. N. Piper, R. I. Ray, A. H. Reed, R. F. L. Self, J. L. Schmidt, S. G. Schock, F. Simonet, R. D. Stoll, D. Tang, D. E. Thistle, E. I. Thorsos, D. J. Walter, and R. A. Wheatcroft, "An overview of SAX99: Environmental considerations," *IEEE J. Oceanic Eng.*, vol. 26, pp. 26–53, Jan. 2001.

[2] N. P. Chotiros, "Biot model of sound propagation in water-saturated sand," *J. Acoust. Soc. Amer.*, vol. 97, pp. 199–214, 1995.

[3] J. L. Lopes, "Observations of anomalous acoustic penetration into sediment at shallow grazing angles," *J. Acoust. Soc. Amer.*, vol. 99, pp. 2473–2474 (A), 1996.

[4] H. J. Simpson and B. H. Houston, "Analysis of laboratory measurements of sound propagating into an unconsolidated water-saturated porous media," *J. Acoust. Soc. Amer.*, vol. 103, pp. 3095–3096, 1998.

[5] A. Maguer, E. Bovio, W. L. J. Fox, E. Pouliquen, and H. Schmidt, "Mechanisms for subcritical penetration into a sandy bottom: Experimental and modeling results," *J. Acoust. Soc. Amer.*, vol. 107, pp. 1215–1225, 2000.

[6] A. N. Ivakin and D. R. Jackson, "Effects of shear elasticity on sea bed scattering: Numerical examples," *J. Acoust. Soc. Amer.*, vol. 103, pp. 346–354, 1998.

[7] D. R. Jackson, personal communication, Applied Physics Laboratory, University of Washington.

[8] E. L. Hamilton, "Attenuation of shear waves in marine sediments," *J. Acoust. Soc. Amer.*, vol. 60, pp. 334–338, 1976.

[9] E. I. Thorsos, D. R. Jackson, J. E. Moe, and K. L. Williams, "Modeling of subcritical penetration into sediments due to interface roughness," in *High Frequency Acoustics in Shallow Water*, N. G. Pace, E. Pouliquen, O. Bergem, and A. P. Lyons, Eds. La Spezia, Italy: NATO SACLANT Undersea Research Centre, 1997, pp. 563–569.

[10] E. I. Thorsos, D. R. Jackson, and K. L. Williams, "Modeling of subcritical penetration into sediments due to interface roughness," *J. Acoust. Soc. Amer.*, vol. 107, pp. 263–277, 2000.

[11] K. L. Williams and D. R. Jackson, "A model for bistatic scattering into ocean sediments for frequencies from 10–100 kHz," Applied Physics Laboratory, Univ. of Washington, APL-UW TR 9505, 1995.
[12] D. Tang, unpublished simulations, Applied Physics Laboratory, Univ. of Washington, Seattle, WA, 1998.
[13] H. J. Simpson and B. H. Houston, "Synthetic array measurements of acoustical waves propagating into a water-saturated sandy bottom for a smoothed and a roughened interface," *J. Acoust. Soc. Amer.*, vol. 107, pp. 2329–2337, 2000.
[14] H. Schmidt and J. Lee, "Physics of 3-D scattering from rippled seabeds and buried targets in shallow water," *J. Acoust. Soc. Amer.*, vol. 105, pp. 1605–1617, 1999.
[15] A. Maguer, E. Bovio, W. L. J. Fox, and H. Schmidt, "In situ estimation of sediment sound speed and critical angle," *J. Acoust. Soc. Amer.*, vol. 108, pp. 987–996, 2000.
[16] E. Pouliquen, A. P. Lyons, and N. G. Pace, "Penetration of acoustic waves into rippled sandy seafloors," *J. Acoust. Soc. Amer.*, vol. 108, pp. 2071–2081, 2000.
[17] R. D. Stoll *et al.*, "Sediment Acoustics," in *Lecture Notes in Earth Sciences*, S. B. Bhattacharji *et al.*, Eds, Berlin: Springer-Verlag, 1989, vol. 26.
[18] B. Gurevich, A. P. Sadovnichaja, S. L. Lopatnikov, and S. A. Shapiro, "Scattering of a compressional wave in a poroelastic medium by an ellipsoidal inclusion," *Geophys. J. Int.*, vol. 133, pp. 91–103, 1998.
[19] D. R. Jackson, K. B. Briggs, K. L. Williams, and M. D. Richardson, "Test of Models for high-frequency sea-floor backscattering," *IEEE J. Oceanic Eng.*, vol. 21, pp. 458–470, 1996.
[20] J. G. Dworski and D. R. Jackson, "Spatial and temporal variation of acoustic backscatter in the STRESS experiment," *Continental Shelf Res.*, vol. 14, pp. 1221–1237, 1994.
[21] D. R. Jackson, K. L. Williams, and K. B. Briggs, "High-frequency acoustic observations of benthic spatial and temporal variability," *Geo-Marine Lett.*, vol. 16, pp. 212–218, 1996.
[22] P. A. Jumars, D. R. Jackson, T. F. Gross, and C. Sherwood, "Acoustic remote sensing of benthic activity: A statistical approach," *Limnol. Oceanogr.*, vol. 41, pp. 1220–1241, 1996.
[23] D. Tang, G. Jin, D. R. Jackson, and K. L. Williams, "Analyzes of high-frequency bottom and subbottom backscattering for two distinct shallow water environments," *J. Acoust. Soc. Amer.*, vol. 96, pp. 2930–2936, 1994.
[24] D. R. Jackson, K. L. Williams, and K. B. Briggs, "High-frequency observations of benthic spatial and temporal variability," *Geomarine Lett.*, vol. 16, pp. 212–218, 1996.
[25] K. B. Briggs and M. D. Richardson, "Small-scale fluctuations in acoustic and physical properties in surficial carbonate sediments and their relationships to bioturbation," *Geomarine Lett.*, vol. 17, pp. 306–315, 1997.
[26] M. D. Richardson and K. B. Briggs, "In-situ and laboratory geoacoustic measurements in soft mud and hard-packed sand sediments: Implications for high-frequency acoustic propagation and scattering," *Geomarine Lett.*, vol. 16, pp. 196–203, 1996.
[27] M. D. Richardson, D. K. Young, and K. B. Briggs, "Effects of hydrodynamic and biological processes on sediment geoacoustic properties in Long Island Sound, USA," *Marine Geol.*, vol. 52, pp. 201–226, 1983.
[28] D. R. Jackson and K. B. Briggs, "High-frequency bottom scattering: Roughness vs. sediment volume scattering," *J. Acoust. Soc. Amer.*, vol. 92, pp. 962–977, 1992.
[29] T. K. Stanton, D. Chu, P. H. Wiebe, R. L. Eastwood, and J. D. Warren, "Acoustic scattering by benthic and planktonic shelled animals," *J. Acoust. Soc. Amer.*, vol. 108, pp. 535–550, 2000.
[30] T. K. Stanton, "On acoustic scattering by a shell-covered seafloor," *J. Acoust. Soc. Amer.*, vol. 108, pp. 551–555, 2000.
[31] L. Zhang, "High Frequency Seafloor Backscattering with the presence of Turbulence in Seawater," Ph.D. dissertation, University of Southern Mississippi, 1996.
[32] E. L. Hamilton, "Geoacoustic Modeling of the Sea Floor," *J. Acoust. Soc. Amer.*, vol. 68, pp. 1313–1340, 1980.
[33] A. W. Nolle, W. A. Hoyer, J. F. Mifsud, W. R. Runyan, and M. B. Ward, "Acoustical properties of water-filled sands," *J. Acoust. Soc. Amer.*, vol. 35, pp. 1394–1408, 1963.
[34] D. J. Wingham, "The dispersion of sound in sediment," *J. Acoust. Soc. Amer.*, vol. 78, pp. 1757–1760, 1985.
[35] N. P. Chotiros, R. A. Altenburg, and J. Piper, "Analysis of acoustic backscatter in the vicinity of the Dry Tortugas," *Geomarine Lett.*, vol. 17, pp. 325–334, 1997.
[36] D. E. Smith, "Localization in nonuniform media: Exponential decay of the late-time Ginzburg-Landau impulse response," *Phys. Rev. B*, vol. 58, pp. 5346–5366, 1998.
[37] R. Lim, J. L. Lopes, R. H. Hackman, and D. G. Todoroff, "Scattering by objects buried in underwater sediments: Theory and experiment," *J. Acoust. Soc. Amer.*, vol. 93, pp. 1762–1783, 1993.
[38] R. Lim, K. L. Williams, and E. I. Thorsos, "Acoustic scattering by a three-dimensional elastic object near a rough surface," *J. Acoust. Soc. Amer.*, vol. 107, pp. 1246–1262, 2000.
[39] L. J. Cutrona, "Comparison of sonar system performance achievable using synthetic-aperture techniques with nonsynthetic-aperture sonar systems," *J. Acoust. Soc. Amer.*, vol. 58, pp. 336–348, 1975.
[40] D. W. Hawkins, "Synthetic Aperture Imaging Algorithms: with application to wide bandwidth sonar," Ph.D. Dissertation, University of Canterbury, Christchurch, New Zealand, 1996.
[41] J. L. Lopes, I. C. Paustian, R. Marciniak, and D. L. Folds, "Dual-Frequency Acoustic Lens Sonar System Development for the Detection of Both Buried Objects and Objects Proud of the Bottom," in *Proc. SPIE AeroSense99*, Orlando, FL, Apr. 1999.

Eric I. Thorsos received the B.S. degree in physics from Harvey Mudd College, Claremont, CA, in 1965, the M.S. degree in engineering and applied science from the University of California at Davis-Livermore in 1966, and the Ph.D. degree in theoretical nuclear physics from the Massachusetts Institute of Technology, Cambridge, in 1972.

From 1972 to 1975, he was an Assistant Professor of Physics at Hobart and William Smith Colleges, Geneva, NY. From 1975 to 1980, he worked in the area of inertial confinement fusion at the Laboratory for Laser Energetics at the University of Rochester, Rochester, NY, and, since 1980, he has worked in underwater acoustics at the Applied Physics Laboratory, University of Washington, Seattle. He is presently a Principal Physicist at the Applied Physics Laboratory and a Research Associate Professor with the Electrical Engineering Department, University of Washington. His research interests include acoustic scattering from the sea surface and the sea bottom, and he was Chief Scientist on SAX99.

Dr. Thorsos is a fellow of the Acoustical Society of America and received the Bronze Medal from the National Defense Industrial Association in 1999.

Kevin L. Williams, photograph and biography not available at the time of publication.

Nicholas P. Chotiros (A'89), photograph and biography not available at the time of publication.

James T. Christoff, photograph and biography not available at the time of publication.

Kerry W. Commander (M'89), photograph and biography not available at the time of publication.

Charles F. Greenlaw, photograph and biography not available at the time of publication.

D. Vance Holliday, photograph and biography not available at the time of publication.

Darrell R. Jackson, photograph and biography not available at the time of publication.

Joseph L. Lopes, photograph and biography not available at the time of publication.

Duncan E. McGehee, photograph and biography not available at the time of publication.

John E. Piper, photograph and biography not available at the time of publication.

Michael D. Richardson, photograph and biography not available at the time of publication.

Dajun Tang, photograph and biography not available at the time of publication.